Article

Cell Reports

Degree of Tissue Differentiation Dictates Susceptibility to BRAF-Driven Colorectal Cancer

Graphical Abstract

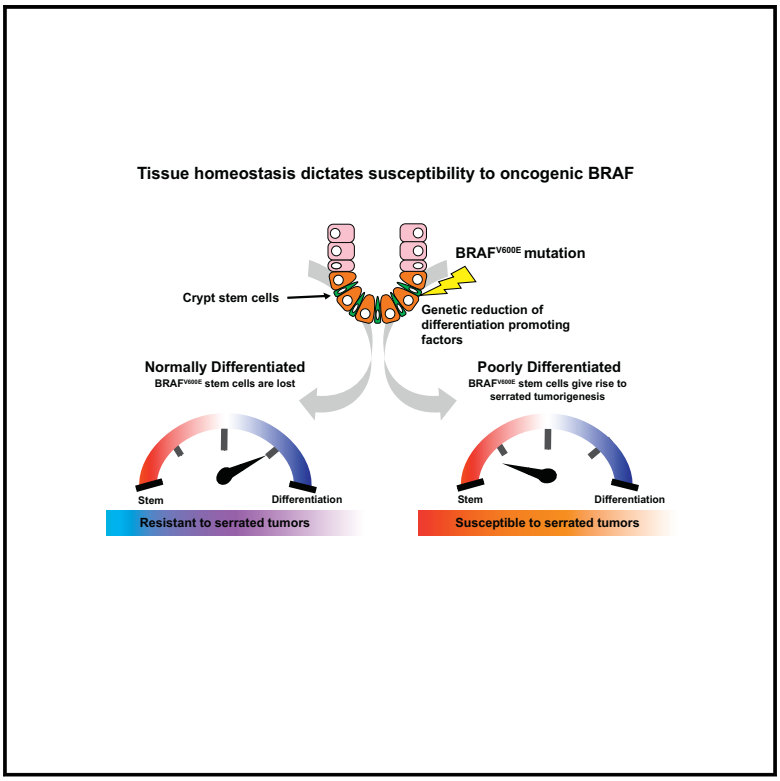

Authors

Kevin Tong, Oscar Pellón-Cárdenas, Veerin R. Sirihorachai, ..., Lanjing Zhang, Jinchuan Xing, Michael P. Verzi

Correspondence

verzi@biology.rutgers.edu

In Brief

Despite high frequency in serrated colon tumors, BRAF^{V600E} inefficiently drives tumorigenesis in mouse models, and paradoxically, BRAF^{V600E} triggers stem cell loss. BRAF-driven tumorigenesis increases in genetic models that reduce differentiation and restore stem cell activity. These findings provide insights into the mechanisms of BRAF^{V600E}-driven colon cancer initiation.

Highlights

- BRAF^{V600E} poorly initiates colon cancer, instead triggering tissue differentiation
- BRAF^{V600E} causes stem cell loss; reduced differentiation restores stem cells
- Mutations that reduce differentiation permit BRAF-driven serrated tumorigenesis
- Patients with reduced differentiation exhibit higher serrated tumor susceptibility

Data and Software Availability

GSE106330
GSE102171
GSE76987

Tong et al., 2017, Cell Reports *21*, 3833–3845
December 26, 2017
https://doi.org/10.1016/j.celrep.2017.11.104

CellPress

Cell Reports
Article

Degree of Tissue Differentiation Dictates Susceptibility to BRAF-Driven Colorectal Cancer

Kevin Tong,[1,2,5] Oscar Pellón-Cárdenas,[1,2,5] Veerin R. Sirihorachai,[1,6] Bailey N. Warder,[1] Om A. Kothari,[1] Ansu O. Perekatt,[1,2] Emily E. Fokas,[1] Robert L. Fullem,[1,7] Anbo Zhou,[1] Joshua K. Thackray,[1] Hiep Tran,[3] Lanjing Zhang,[2,4] Jinchuan Xing,[1] and Michael P. Verzi[1,2,8,*]

[1]Department of Genetics, Rutgers University, Human Genetics Institute of New Jersey (HGINJ), 145 Bevier Road, Piscataway Township, NJ 08854, USA
[2]Rutgers Cancer Institute of New Jersey (CINJ), 195 Little Albany Street, New Brunswick, NJ 08903, USA
[3]Waksman Institute, Rutgers University, Piscataway, NJ 08854, USA
[4]Department of Pathology, University Medical Center of Princeton, Plainsboro, NJ 08536, USA
[5]These authors contributed equally
[6]Present address: Department of Cancer Biology, University of Michigan, 109 Zina Pitcher Place, Ann Arbor, MI 48109, USA
[7]Present address: National Human Genome Research Institute (NHGRI), 5635 Fishers Lane, Rockville, MD 20892, USA
[8]Lead Contact
*Correspondence: verzi@biology.rutgers.edu
https://doi.org/10.1016/j.celrep.2017.11.104

SUMMARY

Oncogenic mutations in BRAF are believed to initiate serrated colorectal cancers; however, the mechanisms of BRAF-driven colon cancer are unclear. We find that oncogenic BRAF paradoxically suppresses stem cell renewal and instead promotes differentiation. Correspondingly, tumor formation is inefficient in BRAF-driven mouse models of colon cancer. By reducing levels of differentiation via genetic manipulation of either of two distinct differentiation-promoting factors (*Smad4* or *Cdx2*), stem cell activity is restored in $BRAF^{V600E}$ intestines, and the oncogenic capacity of $BRAF^{V600E}$ is amplified. In human patients, we observe that reduced levels of differentiation in normal tissue is associated with increased susceptibility to serrated colon tumors. Together, these findings help resolve the conditions necessary for BRAF-driven colon cancer initiation. Additionally, our results predict that genetic and/or environmental factors that reduce tissue differentiation will increase susceptibility to serrated colon cancer. These findings offer an opportunity to identify susceptible individuals by assessing their tissue-differentiation status.

INTRODUCTION

Colorectal cancer (CRC) arises from diverse mutations of oncogenes and tumor suppressors that ultimately traverse a limited set of defined routes to tumorigenesis (Fearon and Vogelstein, 1990; Rad et al., 2013). The majority of colorectal tumors follow a conventional pathway that is initiated by activating mutations of the WNT pathway (Powell et al., 1992). However, at least 5%–10% of CRCs are believed to initiate via activating mutations in the *BRAF* oncogene, which amplifies MAPK signaling and drives the serrated neoplastic pathway to CRC. Serrated tumors are characterized by a sawtooth pattern of epithelial infolding, with additional histological features according to three distinct tumor categories: hyperplastic polyps (HPs), sessile serrated adenomas (SSAs), and traditional serrated adenomas (TSAs) (Rex et al., 2012). Serrated CRC, although less frequent than WNT-driven CRC, carries a worse prognosis (De Sousa E Melo et al., 2013) and is less understood.

The intestinal mucosa is a continuously self-renewing tissue that is organized into defined crypt-villus units: Crypts of Lieberkühn are epithelial pockets tucked into the intestinal wall and contain proliferating stem cells, which feed differentiated progeny onto villi. Villi are luminal projections composed of post-mitotic, differentiated epithelium (Clevers, 2013). Intestinal stem cells are thought to be a key contributor to tumor initiation. Recent mouse studies using genetic techniques for cell-specific manipulation and cell lineage tracking have identified a population of intestinal stem cells called crypt base columnar cells (Barker et al., 2007) that can serve as the cell of origin of CRC (Barker et al., 2009). While intestinal stem cells are not the only cell capable of serving as the cell of origin (Visvader, 2011), they are by far the most efficient, requiring only a single activating mutation of the WNT/β-catenin pathway—a frequent event associated with the progression of the majority of CRCs, such as *APC* mutations in adenocarcinomas (Clevers and Nusse, 2012; Sekine et al., 2016). Paradoxically, despite a high prevalence among colorectal tumors, ectopic expression of an oncogenic *BRAF* mutant transgene promotes either senescence or differentiation of intestinal stem cells (Carragher et al., 2010; Riemer et al., 2015). Thus, while oncogenic activation of BRAF can eventually lead to tumor formation in mouse models, these tumors are slow to arise (Rad et al., 2013; Sakamoto et al., 2017). Thus, in stark contrast to activating mutations of the WNT pathway, oncogenic BRAF mutations inefficiently trigger tumorigenesis.

Because stem cells are likely the cell of origin of most colon cancers, factors influencing stem cell numbers should influence

tumor incidence. Genetic or environmental factors that influence the homeostatic balance between stem and differentiated cells may therefore be expected to alter susceptibility to CRC. Loss of a differentiation-promoting transcription factor, CDX2, has been associated with BRAF-driven serrated tumor development (Bae et al., 2015; Dalerba et al., 2016; Landau et al., 2014; Sakamoto et al., 2017), although it is still unclear whether CDX2 may function in tumor initiation. SMAD4, a differentiation-promoting transcriptional effector of the transforming growth factor β (TGF-β)/BMP signaling pathway, is inactivated in 10%–15% of CRC (Fearon, 2011), although its role in initiation of serrated tumors has not been functionally explored. Interestingly, both of these transcription factors have been ascribed roles antagonistic to the WNT-signaling pathway (Guo et al., 2010; Liu et al., 2012; Tian et al., 2009). Whether these transcription factors, or the state of tissue differentiation, influences BRAF-driven tumor initiation is still unclear.

In this study, we show that BRAF activation promotes differentiation of the intestinal epithelium, intestinal stem cell loss, and inefficient oncogenesis. However, in genetic backgrounds with reduced levels of the differentiation-promoting transcription factors *Cdx2* or *Smad4*, homeostasis is restored, stem cell activity returns, and oncogenesis ensues at an accelerated pace. Additionally, gene expression analysis of normal human colon tissue indicates an inverse correlation between the differentiation status of the colon mucosa and a patient's susceptibility to serrated tumors. By highlighting oncogenic mechanisms through which BRAF-driven CRC initiates, these observations may directly impact the development of alternative diagnostic and preventative approaches for serrated CRC by directly targeting the homeostatic balance between stem and differentiated cells.

RESULTS

BRAF^{V600E} Inefficiently Drives Tumorigenesis and Promotes Differentiation in a Murine Model of Serrated Colon Cancer

Studies of melanoma and colon tumorigenesis have shown that the *BRAF*^{V600E} oncogene, while a prevalent driver of human cancers, is inefficient in promoting tumorigenesis in model systems (Dhomen et al., 2009; Rad et al., 2013). Mutant BRAF activation triggers cellular senescence in some models (Carragher et al., 2010) and intestinal stem cell differentiation in others (Riemer et al., 2015). A third model only observes p21 expression at later stages of tumor progression (Rad et al., 2013). Differences among these models may be attributed to embryonic versus adult-onset of activation, or varying expression levels of mutant BRAF between models. Using a mouse model not previously employed for studies of BRAF^{V600E}-driven intestinal tumorigenesis, we conditionally activated either one or two alleles of the BRAF oncogene from its endogenous locus (Dankort et al., 2007), specifically within the adult intestinal epithelium using the conditional *Villin-Cre*^{ERT2} driver (el Marjou et al., 2004). 5 days after tamoxifen-induced activation, expression of MAPK target genes (Rad et al., 2013) is increased in *BRAF*$^{V600E/+}$ mice compared to controls (Figure 1A), confirming activation of downstream BRAF signaling. The *BRAF*$^{V600E/+}$ epithelium also took on a more pronounced serrated morphology, a hallmark of serrated colon tumors. To more closely investigate how activation of *BRAF*^{V600E} immediately impacts the epithelium, we probed tissue markers at 5 days after the onset of tamoxifen treatment (Figure 1B). Interestingly, increased stain intensity of the differentiation marker alkaline phosphatase was observed in the *BRAF*$^{V600E/+}$ mutants compared to controls, suggesting a more differentiated epithelium. Conversely, levels of the stem cell marker OLFM4 decreased (Figure 1B). These phenotypic changes were further exacerbated in the *BRAF*$^{V600E/V600E}$ homozygous mutant (from here on indicated as *BRAF*^{V600E}) and suggest that activation of BRAF shifts the stem-differentiation homeostatic balance toward a differentiated cell state (Figure 1B). Transcriptomic changes in the *BRAF*$^{V600E/+}$ epithelium corroborated an increase in differentiation and decrease in stemness in the mutant crypt epithelium. Gene set enrichment analysis (GSEA) (Subramanian et al., 2005) revealed that expression levels of stem cell-specific genes (Muñoz et al., 2012) are significantly reduced in *BRAF*$^{V600E/+}$ mice compared to controls (Figure 1C), consistent with the reduction in OLFM4 staining (Figure 1B). Conversely, expression of differentiation genes (Chong et al., 2009) was increased compared to controls (Figure 1D). We also probed for senescence upon induction of mutant BRAF. Consistent with some previous models of mutant BRAF activation (Riemer et al., 2015), the senescence marker p21 was not expressed upon tamoxifen treatment of *BRAF*$^{V600E/+}$ mice. However, p21 was robustly induced upon activation of two BRAF alleles (Figure 1B). These findings suggest that induction of senescence is a function of BRAF activation levels and may resolve differences between previous studies regarding BRAF-mediated induction of senescence markers in the intestine.

Consistent with the promotion of senescence and cellular differentiation, no tumors were observed in 13 *BRAF*$^{V600E/+}$ mice between 6 and 16 months after tamoxifen treatment, and dysplastic lesions were only observed in 30% of the mice, with no more than 1 lesion observed per affected animal. Taken together, the *Villin-Cre*^{ERT2}*;BRAF*^{V600E} models recapitulate aspects of BRAF-driven human tumorigenesis (including elevated MAPK signaling and serrated histopathology), but inefficiently induce tumors, potentially owing to an imbalance of the stem-differentiation homeostasis in the gut epithelium.

Loss of CDX2 Promotes BRAF-Driven Tumorigenesis by Re-balancing Stem/Differentiation Homeostasis

The imbalance of stem-to-differentiation homeostasis triggered by BRAF^{V600E} may underlie the inefficiency of the BRAF mouse model to drive oncogenesis. Therefore, conditions reducing differentiation may restore homeostatic balance and permit BRAF-driven tumor initiation. CDX2 is a homeodomain transcription factor that promotes differentiation in the intestinal epithelium (Mutoh et al., 2002; Silberg et al., 2002; Suh and Traber, 1996). CDX2 directly binds and activates hundreds of enterocyte target genes, promoting differentiation-related cell functions (Verzi et al., 2010), while loss of CDX2 results in mice that lack complete differentiation of the epithelium (Stringer et al., 2012). Furthermore, reduced expression of CDX2 is associated with BRAF mutant colon cancers (Bae et al., 2015; Dalerba et al., 2016; Landau et al., 2014; Sakamoto et al., 2017). To explore

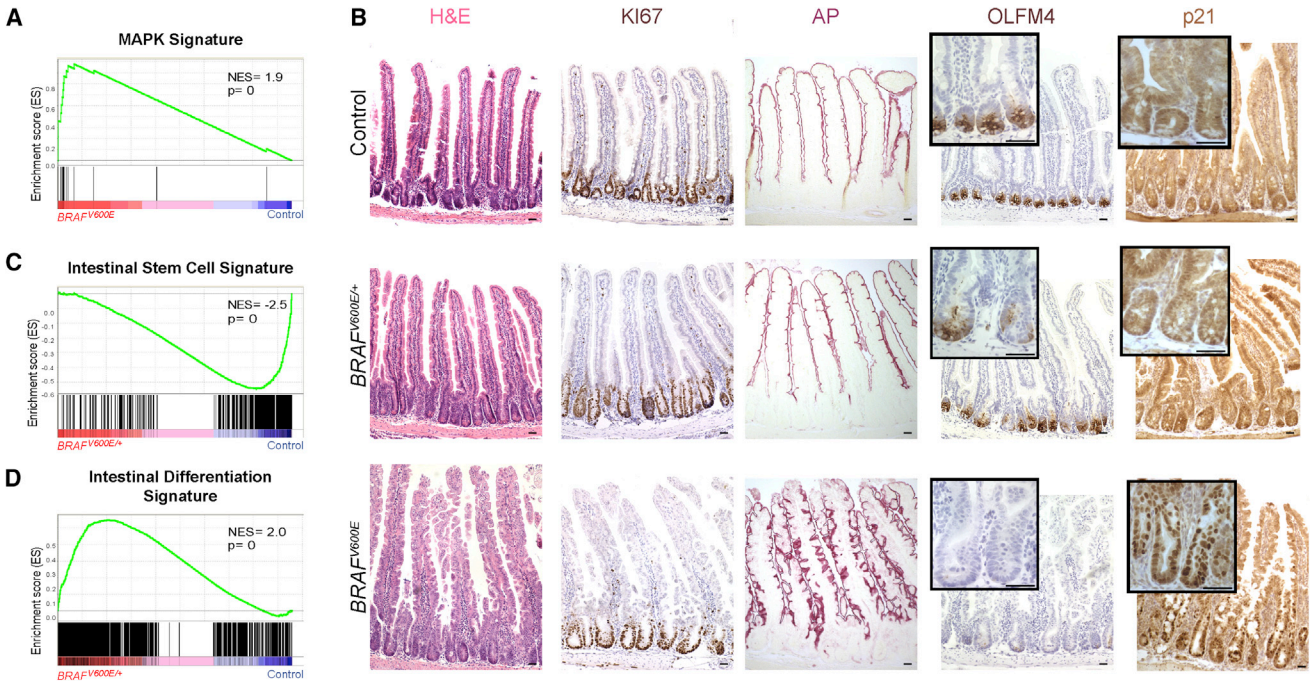

Figure 1. *BRAF*^{V600E} Activation Alters Intestinal Homeostasis, Promoting Differentiation

(A) GSEA analysis reveals that MAPK target genes (Rad et al., 2013), were elevated in the *BRAF*$^{V600E/+}$ mutants, as expected (K-S test).

(B) Assessment of morphological changes (H&E), proliferation (Ki67), differentiation (AP), stem cells (OLFM4), and senescent cells (p21) in *BRAF*$^{V600E/+}$ and *BRAF*$^{V600E/600E}$ mutants. Note increasing levels of differentiation markers and decreasing levels of the stem cell marker with the increased number of activated BRAF alleles. Representative images from 3 biological replicates. Scale bars, 50 μm.

(C and D) (C) Intestinal stem cell gene expression levels are significantly reduced in *BRAF*$^{V600E/+}$ mutants, whereas (D) intestinal differentiation gene signatures are significantly increased compared to controls.

the mechanisms by which CDX2 may modify BRAF^{V600E}-driven tumorigenesis, we generated an allelic series of mutants lacking either one or both copies of *Cdx2* (Verzi et al., 2010), in combination with one or two alleles of activated *BRAF*^{V600E}. As noted before, activation of *BRAF*^{V600E} alleles diminished expression of stem cell markers (Figure 2A). However, simultaneous loss of *Cdx2* alleles in the *BRAF*^{V600E} models restored OLFM4 expression, indicating an increased population of stem cells in the compound mutant relative to the BRAF mutant (Figure 2A). We next assayed for stem cell activity using the organoid formation assay (Sato et al., 2009). Consistent with reduced levels of OLFM4 staining, *BRAF*$^{V600E/+}$ crypts were incapable of giving rise to organoids (Riemer et al., 2015) (Figure 2B). However, organoids could be derived from the *Cdx2*$^{f/+}$; *BRAF*$^{V600E/+}$ animals, indicating that reduction of CDX2 restores stem cell activity that is lost upon activation of *BRAF*^{V600E}. We saw a similar pattern of stem cell reporter activity *in vivo*, using the *Lgr5-GFP-Cre*^{ERT2} reporter line (Barker et al., 2007) to mark Lgr5^{+} stem cells and activating mutations with the *Villin-Cre*^{ERT2} driver. GFP^{+} cells were observed at the crypt base in control and *CDX2*; *BRAF*^{V600E} mutant crypts, but were completely depleted in *BRAF*^{V600E} mutant crypts (Figure 2C). Similarly, using the stem cell-specific *Lgr5-GFP-Cre*^{ERT2} driver (Barker et al., 2007), we assayed for stem cell renewal *in vivo* by monitoring Cre-mediated recombination of *loxP* elements in the engineered *BRAF*^{V600E} locus (Dankort et al., 2007). *BRAF*^{V600E} recombination was not preserved in *Lgr5-Cre*; *BRAF*$^{V600E/+}$mice (Figure 2D), indicating that mutant stem cells could not renew and were depleted over time, presumably replaced by neighboring cells that had not undergone Cre-mediated recombination. By contrast, sustained recombination of *Cdx2*$^{f/+}$; *BRAF*$^{V600E/+}$ alleles in *Lgr5-Cre* expressing stem cells was compatible with stem cell renewal, as recombined cells and their progeny were still present as far as 10 months after treatment, indicating that CDX2 loss restores the ability of Lgr5^{+} stem cells to renew in the presence of *BRAF*^{V600E} (Figure 2D). It is possible that the loss of stem cells upon *BRAF*^{V600E} activation is due to a promotion of apoptosis. However, the immunohistochemical analysis of the apoptosis marker, cleaved-caspase 3 (CC3), revealed no changes (Figure S1A). We also examined cellular senescence as a possible contributor of stem cell loss, using the marker p21. Interestingly, CDX2 loss reversed the upregulation of p21 induced by BRAF^{V600E}. This was observed at the histological level, the transcript level and in organoid cultures (Figures S1B–S1D). Thus, while *BRAF*$^{V600E/+}$ and *BRAF*^{V600E} appears to be incompatible with stem cell self-renewal and retention, the reduction of CDX2 is able to prevent the loss of stem cells in a BRAF^{V600E} background.

If stem cell populations were restored upon CDX2 loss, the differentiation-promoting effects of BRAF^{V600E} may have also reverted in the *Cdx2*$^{f/f}$;*BRAF*^{V600E} compound mutant mice. To assess the differentiation status of the *Cdx2*$^{f/f}$;*BRAF*^{V600E} mice,

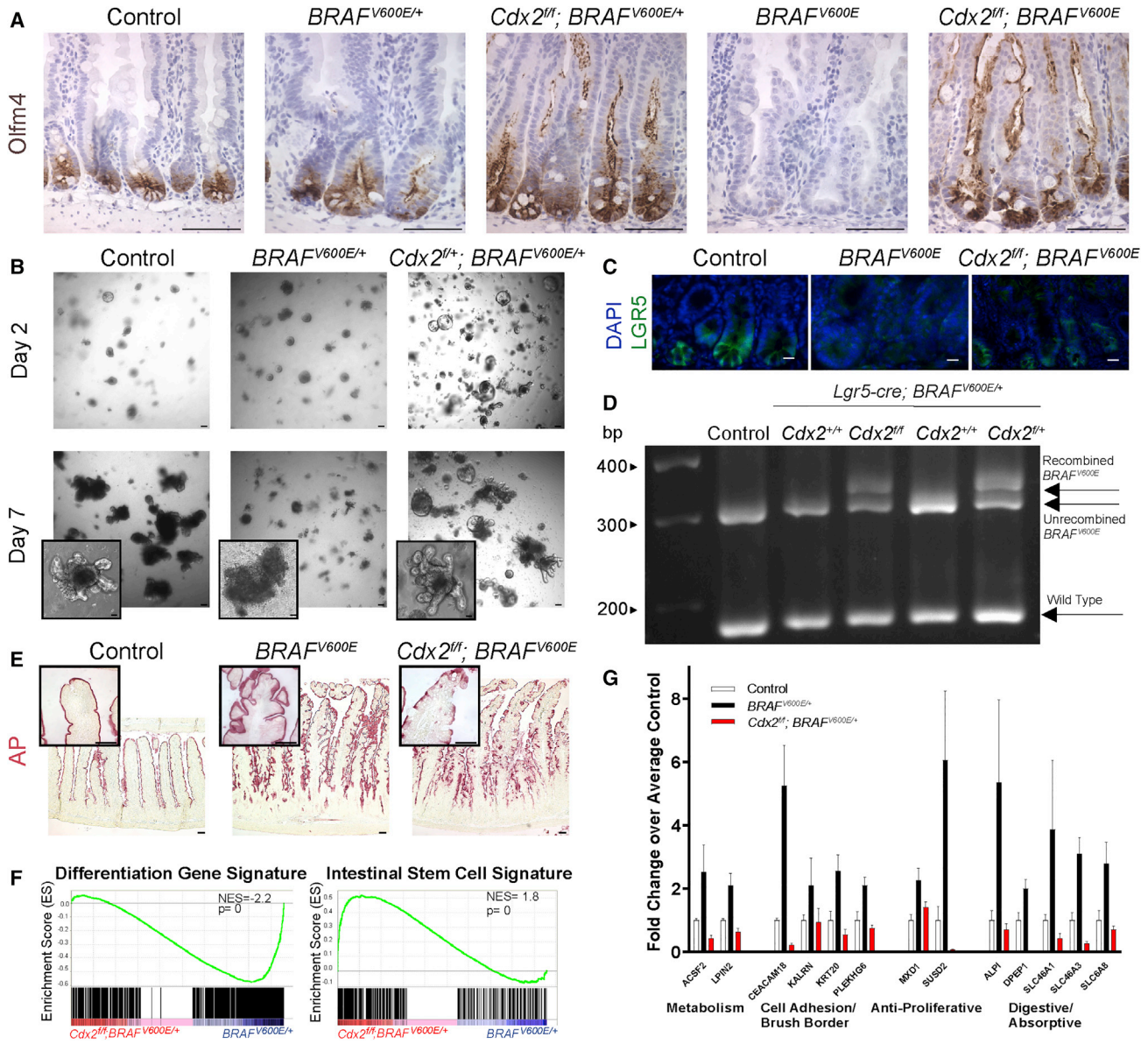

Figure 2. Ablation of CDX2 Reverses BRAF^{V600E}-Driven Changes in Stem/Differentiation Homeostasis

(A) Immunohistochemistry of OLFM4 in uninjected control, *BRAF*$^{V600E/+}$, *Cdx2*$^{f/f}$;*BRAF*$^{V600E/+}$, *BRAF*^{V600E}, and *Cdx2*$^{f/f}$;*BRAF*^{V600E} mice, 5 days post-tamoxifen treatment.

(B) Primary organoid cultures isolated from control, *BRAF*$^{V600E/+}$, and *Cdx2*$^{f/+}$;*BRAF*$^{V600E/+}$ mice. *BRAF*$^{V600E/+}$ mutant cells do not give rise to viable organoids, but reduction of CDX2 levels permits their growth. Representative of 3 biological replicates. Scale bars, 50 μm.

(C) Lgr5-GFP expression. Scale bars, 50 μm.

(D) Recombination at the *BRAF*^{V600E} locus, induced by tamoxifen treatment of the stem cell-specific, conditional Cre (*Lgr5-*^{CreERT2}*-IRES-eGFP*), is not sustained unless *Cdx2* is simultaneously inactivated in the stem cells. Samples from crypt epithelium were harvested at 2 days or 10 months after tamoxifen treatment.

(E) AP staining reveals increased expression in *BRAF*$^{V600E/+}$ and *BRAF*^{V600E}, which is reduced when *Cdx2* is lost.

(F) GSEA shows intestinal stem cell genes are elevated while differentiation genes are reduced upon loss of CDX2, reversing gene expression changes induced by *BRAF*^{V600E} activation.

(G) Examples of the types of differentiation-associated genes that are elevated upon BRAF activation and suppressed upon CDX2-loss. Bars represent mean ± SD from three independent experiments for control and *BRAF*$^{V600E/+}$ and two independent experiments for *Cdx2; BRAF*$^{V600E/+}$.

alkaline phosphatase activity was assayed. Consistent with a restoration of the stem-differentiation balance in the compound mutant epithelium, reduced levels of alkaline phosphatase were observed in the compound *Cdx2*$^{f/f}$*; BRAF*^{V600E} mutants relative to single mutant animals (Figure 2E). These observations were mirrored in transcriptome analyses, which revealed a significant

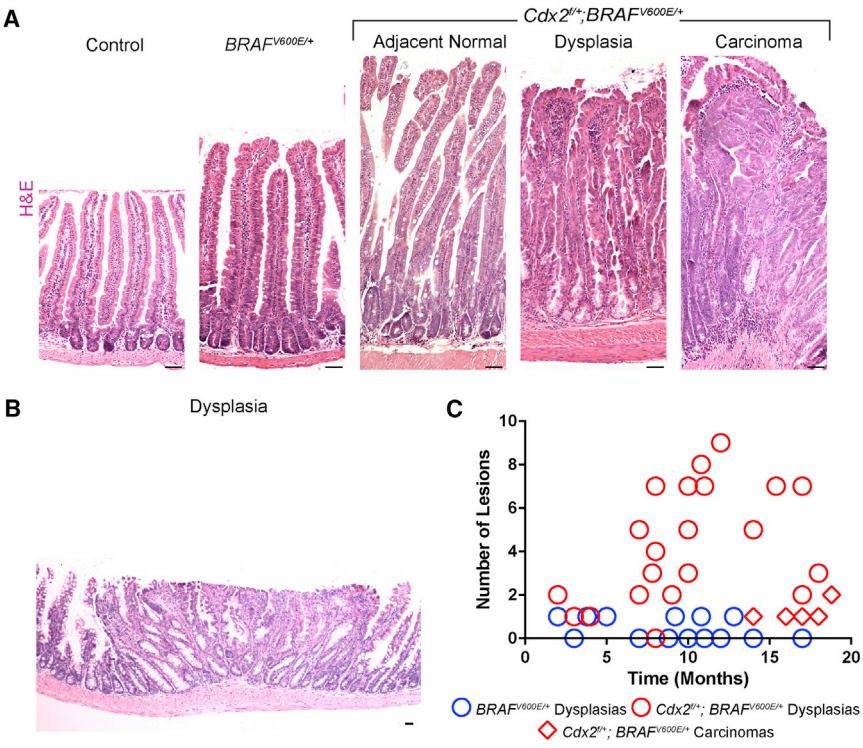

Figure 3. Loss of CDX2 Accelerates BRAF-Driven Tumorigenesis

(A) H&E stains of age-matched control, $BRAF^{V600E/+}$, and $Cdx2^{f/+}$;$BRAF^{V600E/+}$ mice reveal characteristics of serrated cancer morphologies. Dysplasia and carcinomas had characteristics of human hyperplastic polyps (HPPs), SSAs, and serrated carcinomas. See also Figure S3.

(B) More serrated lesions were found in $Cdx2^{f/+}$; $BRAF^{V600E/+}$ compound mice than age-matched $BRAF^{V600E/+}$ counterparts. Counts were based upon complete Swiss roll sections. Scale bars, 50 μm.

elevation of stem cell and reduction of differentiation gene expression levels in the $Cdx2^{f/f}$; $BRAF^{V600E/+}$ epithelium compared to the $BRAF^{V600E/+}$ single mutant (Figure 2F). A wide array of transcripts associated with differentiation were elevated in the $BRAF^{V600E/+}$ epithelium and restored to normal levels upon inactivation of *Cdx2*, including transcripts associated with metabolism, cell adhesion, and digestive/absorptive functions (Figure 2G). Paneth cells, which function in part by supporting the stem cell niche, are diminished in the $BRAF^{V600E/+}$ epithelium. However, lysozyme staining reveals that $CDX2^{f/f}$;$BRAF^{V600E}$ mice show similar loss of lysozyme staining at the crypt base, suggesting that stem cell regulation is not dependent on Paneth cells in this model, as has been established in other models of Paneth cell loss (Durand et al., 2012; Kabiri et al., 2014; Kim et al., 2012) (Figure S2).

Because reduced levels of differentiation-promoting CDX2 allowed retention of stem cells in the $BRAF^{V600E}$ condition, reduced CDX2 levels might also lead to increased tumorigenesis in the $Cdx2^{f/+}$; $BRAF^{V600E/+}$ model. When compared to controls, the histology of the intestinal epithelium is dramatically altered in age-matched $BRAF^{V600E/+}$ and $Cdx2^{f/+}$; $BRAF^{V600E/+}$ compound mutants (Figures 3A and S3). Both the $BRAF^{V600E/+}$ and $Cdx2^{f/+}$; $BRAF^{V600E/+}$ mice exhibited jagged, undulating epithelium, a hallmark of serrated tumors (Leggett and Whitehall, 2010) that is not observed in control or $Cdx2^{f/f}$;$Vil\text{-}Cre^{ERT2}$ mutant mice (Verzi et al., 2010). Dysplastic lesions in $Cdx2^{f/+}$; $Braf^{V600E/+}$ mice were broad with a low profile (Figure 3B). While dysplastic characteristics of SSA were found in both mutant strains of mice, serrated lesions were found more frequently in $Cdx2^{f/+}$; $Braf^{V600E/+}$ mice than in the $Braf^{V600E/+}$ mice (Figure 3C), and macroscopic tumors were found exclusively in $Cdx2^{f/+}$; $Braf^{V600E/+}$ mutants. These flat tumors exhibited a cloud-like surface without discernible borders, similar to endoscopic features of human precursor SSAs (Hazewinkel et al., 2013). Histopathology of $Cdx2^{f/+}$; $Braf^{V600E/+}$ carcinomas revealed significant muscle infiltration, epithelial serrations, eosinophilic cytoplasm, vesicular nuclei, and in some cases, excessive mucin production (Figures 3A and S3). Serrated polyps detected in $Cdx2^{f/+}$; $Braf^{V600E/+}$ compound mutant mice mainly resembled human hyperplastic polyps and sessile serrated adenomas (Figures 3A and S3). The "hyperplastic polyps" were either of the goblet cell type or the microvesicular type and had a saw-tooth configuration with pleomorphic nuclei, while "sessile serrated polyps" showed significant dilated crypts with mature mucinous cells (Figure S3). These findings indicate that reduced levels of *Cdx2* restore the disrupted stem-differentiation balance caused by activation of $BRAF^{V600E}$ and create a permissive environment for the oncogenic $BRAF^{V600E}$ mutation. Importantly, aside from increased susceptibility to BRAF-driven tumors, $Cdx2^{f/+}$ mutants are otherwise healthy and indistinguishable from littermate controls. This raises the possibility that reduced levels of differentiation in otherwise healthy individuals could underlie susceptibility to serrated neoplasia.

The Differentiation-Promoting Factor SMAD4 Also Antagonizes BRAF-Driven Tumorigenesis and Alters the Stem-Differentiation Homeostatic Balance

To further explore whether an imbalance in stem-to-differentiation homeostasis can increase susceptibility to serrated tumors, we tested whether another differentiation-promoting factor could modify tumor initiation of the $BRAF^{V600E/+}$ model. The critical role of SMAD4 in the TGFβ/BMP signaling pathway prompted us to consider it a prime candidate, as TGF-β/BMP signaling is a known promoter of intestinal differentiation. We bred *Smad4* conditional alleles (Yang et al., 2002) into the $BRAF^{V600E/+}$ mutant and found suppression of alkaline phosphatase activity (Figure 4A) and a concomitant increase in the stem cell markers OLFM4 and Lgr5-GFP (Figures 4B and 4C). Stem cell activity was also restored in the context of the organoid forming assay

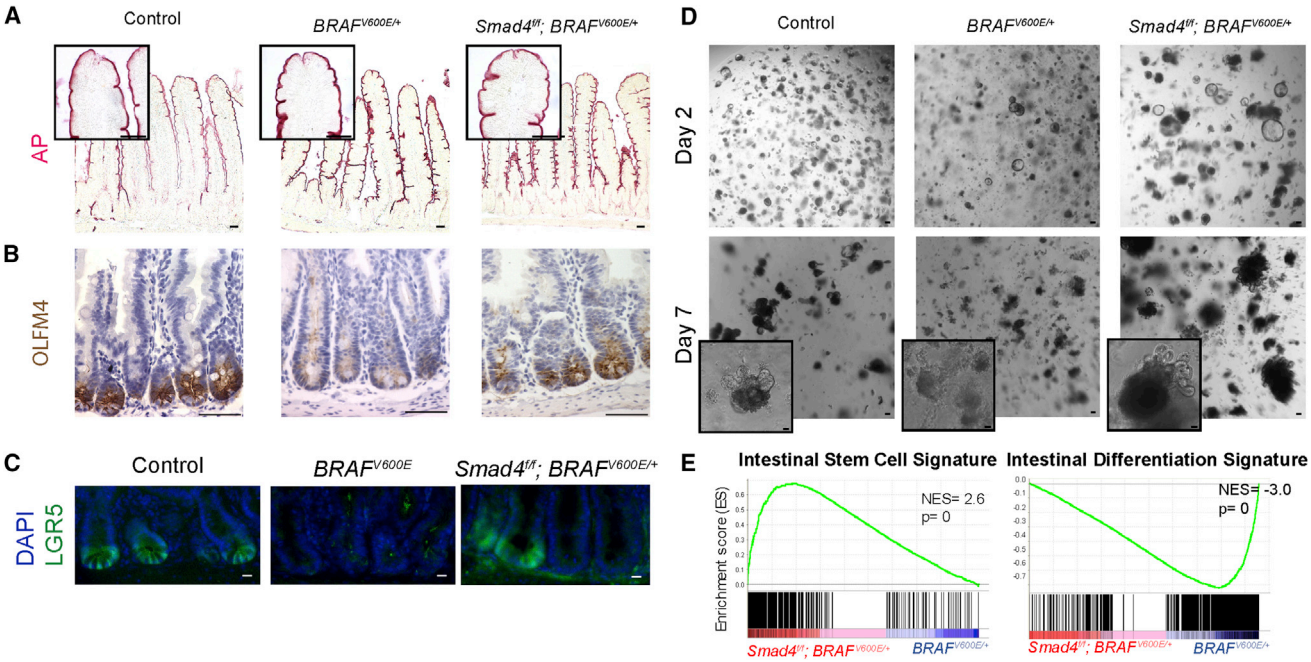

Figure 4. Loss of SMAD4 Restores the Stem-Differentiation Balance that Is Altered upon *BRAF*$^{V600E/+}$ Activation

Figure360▷ For a Figure360 author presentation of Figure 4, see the figure legend at https://doi.org/10.1016/j.celrep.2017.11.104.

(A) AP staining reveals that *Smad4* loss reverses the increase in differentiation induced by *BRAF*$^{V600E/+}$.

(B) OLFM4 staining suggests that loss of SMAD4 in *BRAF*$^{V600E/+}$ tissue reverses stem cell loss. Representative of 3 biological replicates. Scale bars, 50 μm.

(C) Lgr5-GFP expression is lost upon BRAF^{V600E} expression but restored upon SMAD4-loss.

(D) Organoid cultures isolated from control, *BRAF*$^{V600E/+}$, and *Smad4*$^{f/f}$;*BRAF*$^{V600E/+}$ mice reveal a rescue in viability in *Smad4*$^{f/f}$;*BRAF*$^{V600E/+}$ organoids.

(E) GSEA shows intestinal differentiation genes are reduced, while stem cell gene expression is elevated upon loss of SMAD4, reversing gene expression changes induced by *BRAF*$^{V600E/+}$ activation.

(Figure 5D) when SMAD4 loss was combined with *BRAF*$^{V600E/+}$. Again, transcriptomic analysis of *BRAF*$^{V600E/+}$ versus *Smad4*$^{f/f}$;*BRAF*$^{V600E/+}$ compound mutants revealed a shift in gene expression, with an increase in expression of stem cell signature genes and a decrease of differentiated cell gene expression (Figure 4E). Recapitulating the histological analysis, the expression of differentiation genes, such as *Alpi* and *Krt20*, were significantly higher upon *BRAF*^{V600E} activation, but were restored to near normal levels upon simultaneous loss of SMAD4 (Figure S4, ANOVA, $p < 0.05$). Taken together, reduction of SMAD4 restores the stem-to-differentiation balance of the intestinal epithelium that is shifted toward differentiation upon activation of *BRAF*^{V600E}. Thus, two independent genetic models show that reduced levels of differentiation-promoting factors can restore the homeostatic balance between stem and differentiated cells that is disrupted upon *BRAF*^{V600E} activation.

Akin to our findings from the *Cdx2* study described above, the *Smad4*$^{f/f}$;*BRAF*$^{V600E/+}$ compound mutant exhibited increased susceptibility to serrated tumors—including serrated dysplastic regions and invasive carcinomas (Figures 5A, 5B, and S5). Large visible tumors were seen within the intestinal tract as early as 2–3 months post-tamoxifen injection (Figure 5C). Furthermore, as early as 1 month post-tamoxifen treatment, dysplastic lesions were observed in the compound mutants, while carcinomas were found as early as 3 months post-treatment. Thus, loss of a differentiation promoting transcription factor SMAD4, like CDX2, results in an alteration of the stem/differentiation balance in the intestinal epithelium and corresponds to increased BRAF-driven tumor susceptibility.

Elevated WNT Signaling Is Common to Both Genetic Models and Can Rescue Stem Cell Loss in BRAF Mutant Mice

To elucidate a mechanism through which reduced levels of differentiation factors can predispose to serrated tumorigenesis, we explored common transcriptomic signatures of epithelia expressing activated *BRAF*$^{V600E/+}$ and inactivating mutations of either *Cdx2* or *Smad4.* In both cases, WNT signature genes (Van der Flier et al., 2007) were significantly elevated in these models' transcriptomes (Figure 6A). A panel of commonly studied WNT-target genes exemplify these findings (Figure 6B). Notably, just as SMAD4 or CDX2 loss can restore organoid-forming ability of the *BRAF*^{V600E} epithelium, addition of WNT ligand (WNT3A), a WNT-pathway agonist (CHIR-98014), or genetic activation of the WNT pathway (Harada et al., 1999) rescues the organoid forming potential of the *BRAF*$^{V600E/+}$ mutants (Figure 6C). These findings indicate that elevation of the WNT signaling pathway, which functions to promote stem/proliferation in the intestinal epithelium, restores stem cell activity that is normally antagonized by the *BRAF*^{V600E} oncogene. Consistent with these observations, immunohistochemical staining for the WNT target gene products SOX9 and CD44 were elevated

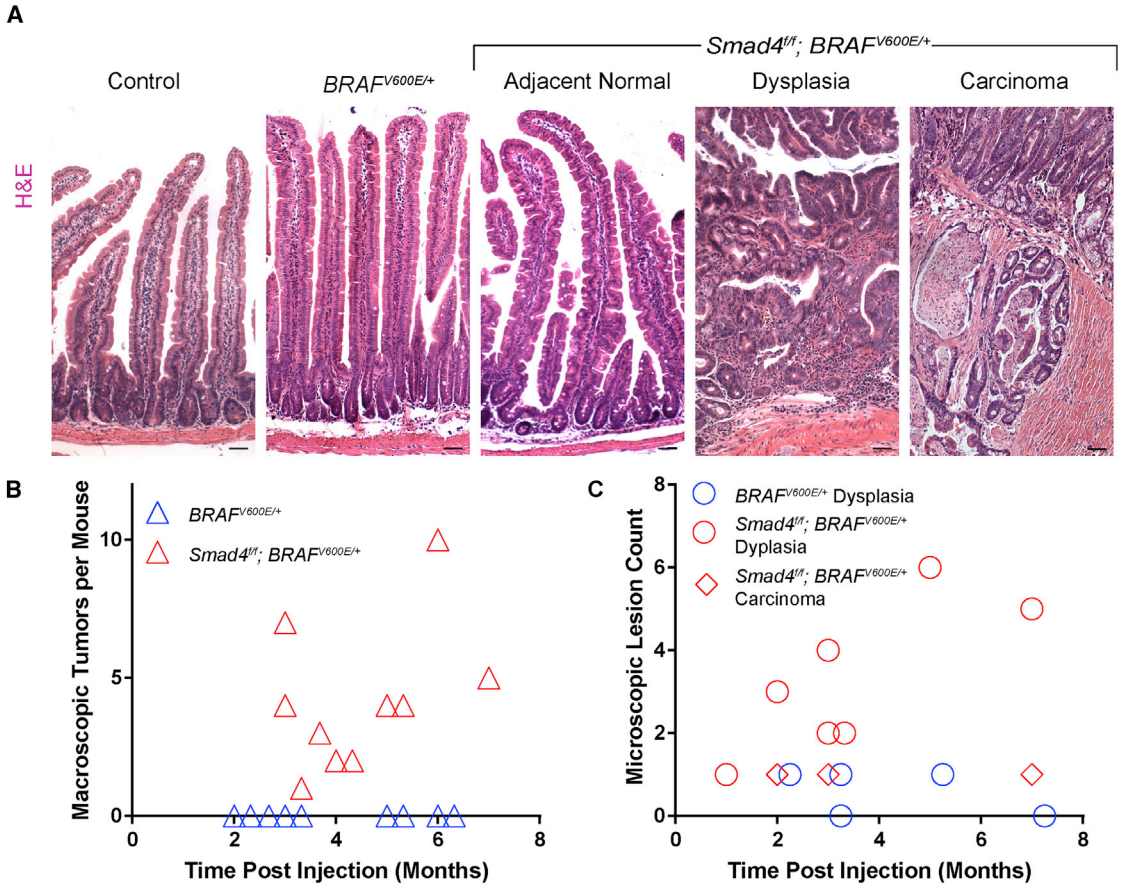

Figure 5. Tumorigenesis in *BRAF*$^{V600E/+}$ Mice Is Accelerated upon the Loss Smad4

(A) H&E stain shows overall morphology of adjacent normal and tumor regions of the intestine of control, *BRAF*$^{V600E/+}$, and *Smad4*$^{f/f}$;*BRAF*$^{V600E/+}$ mice. Similar to *Cdx2*$^{f/+}$;*BRAF*$^{V600E/+}$ mice, dysplasia and carcinomas featured serrated morphologies. See also Figure S5.

(B and C) Counts of macroscopic (B) and microscopic (C) lesions observed in *BRAF*$^{V600E/+}$ mice are lower than *Smad4*$^{f/f}$;*BRAF*$^{V600E/+}$ mutants. Scale bars, 50 μm.

upon loss of either *Cdx2* or *Smad4* (Figure 6D). Finally, to test whether the loss of *Cdx2* or *Smad4* rescues BRAF^{V600E}-organoid forming ability via a WNT-dependent mechanism, we inhibited the WNT pathway using the chemical inhibitors IWP-2 or XAV-939, which block WNT secretion or β-catenin stabilization, respectively. These WNT-pathway inhibitors each reverse the effects of SMAD4 and CDX2 loss, indicating that the rescue of stem cell activity in the organoid forming assay is dependent upon WNT signaling (Figure 6E).

This work suggests a diminished state of epithelial differentiation is required for oncogenic mutations of *BRAF* to be sustained and promote serrated tumorigenesis. We observe that 3 different regulators of the stem-to-differentiated transition of the intestinal epithelium can critically influence the potential of BRAF-driven oncogenesis to sustain stemness in the organoid-forming assay.

Expression of Differentiation Genes in the Human Epithelium Correlates with Susceptibility to Serrated Tumorigenesis

Given that an epithelium with reduced capacity for differentiation (*Smad4*$^{f/f}$ *or Cdx2*$^{f/+}$) predisposed the murine epithelium to BRAF^{V600E}-oncogenesis, we investigated whether differentiation status corresponds to serrated tumor susceptibility. Normal tissue from serrated tumor patients is not abundant in the literature, as most studies focus on tumor tissues. Fortunately, a recent study performed transcriptional profiling from mucosal biopsies of non-tumor tissues from the right colons of serrated tumor patients and control individuals (Delker et al., 2014; Kanth et al., 2016). We queried these data to determine whether the differentiation genes that were reduced in pre-neoplastic tissue of our murine models (Figures 2F and 4F) are also reduced in the normal epithelium of patients exhibiting one (sporadic) or multiple (syndromic) serrated tumors. Interestingly, serrated cancer patients exhibited significantly reduced expression of intestinal differentiation genes in their normal tissues when compared to control patients (Figure 7A). We next applied a k-clustering approach to determine whether patients could be accurately classified into tumor and normal subject groups based upon changes in their stem and differentiation gene expression levels. K-means clustering on 1,000 random gene panels of equal size to our gene lists provides a baseline distribution of clustering accuracies by chance alone (measured by Rand index [RI], median

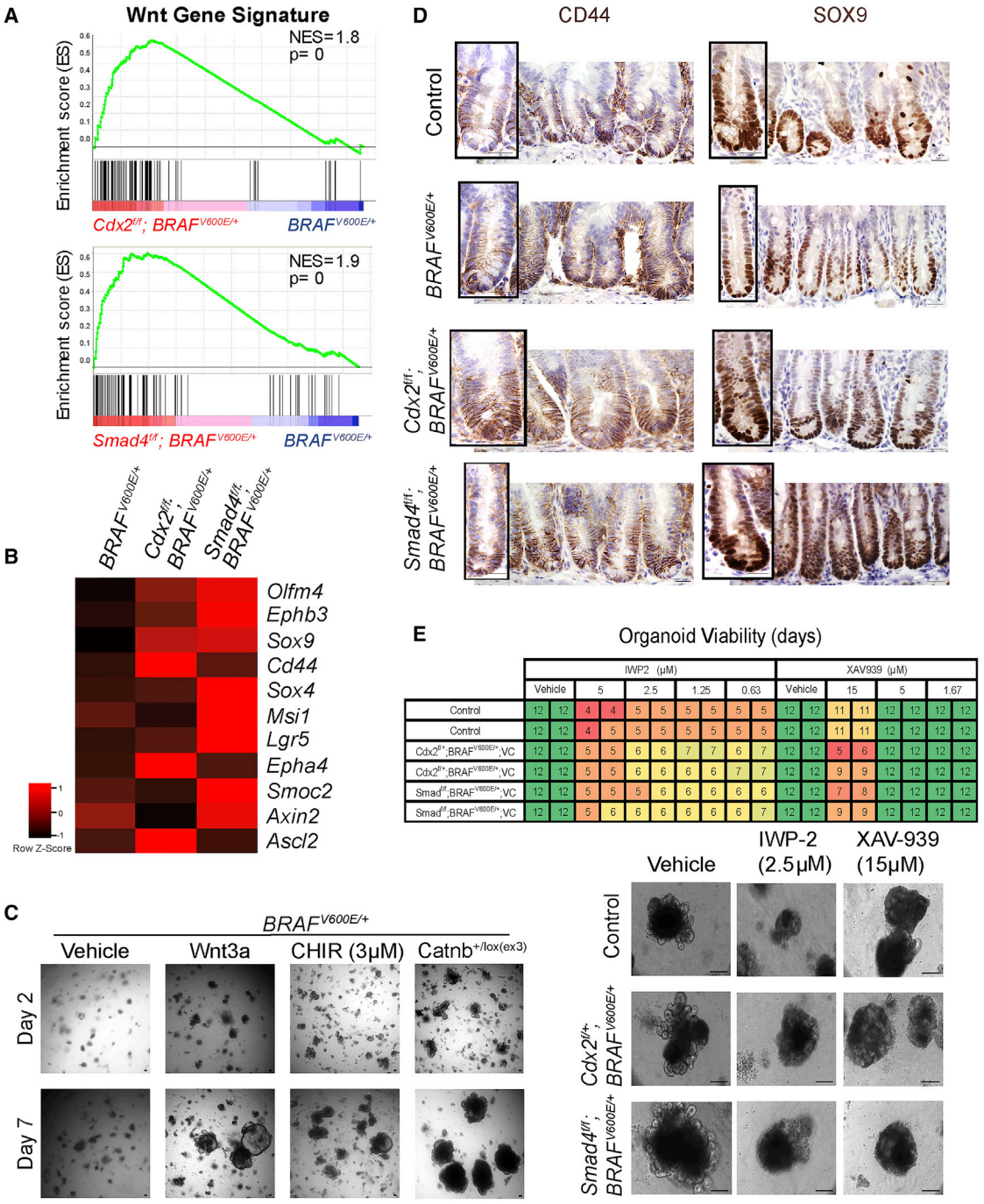

Figure 6. Elevated WNT Signaling May Restore Oncogenic Potential in *Cdx2*$^{f/f}$;*BRAF*$^{V600E/+}$ and *Smad4*$^{f/f}$;*BRAF*$^{V600E/+}$ Double Mutant Mice

(A) Transcriptome analysis of WNT signature genes (Van der Flier et al., 2007) indicates increased WNT target gene expression in the double mutant mice when compared to *BRAF*$^{V600E/+}$ mice (K-S test).

(B) Common intestinal WNT target genes are highlighted.

(C) Organoid cultures derived from *BRAF*$^{V600E/+}$ crypts survive when treated with either WNT3A or the WNT-pathway agonist CHIR-98014.

(D) Immunohistochemistry of WNT targets CD44 and SOX9 show elevated levels in *Cdx2*$^{f/f}$;*BRAF*$^{V600E/+}$ and *Smad4*$^{f/f}$;*BRAF*$^{V600E/+}$ mutants compared to *BRAF*$^{V600E/+}$ mutants.

(E) Organoid cultures derived from compound mutant mice show sensitivity to WNT inhibitors. Table describes viability in days of mature organoids after treatment with XAV-939 or IWP-2. Representative of 2 biological replicates and 3 technical replicates each. Scale bars, 50 μm.

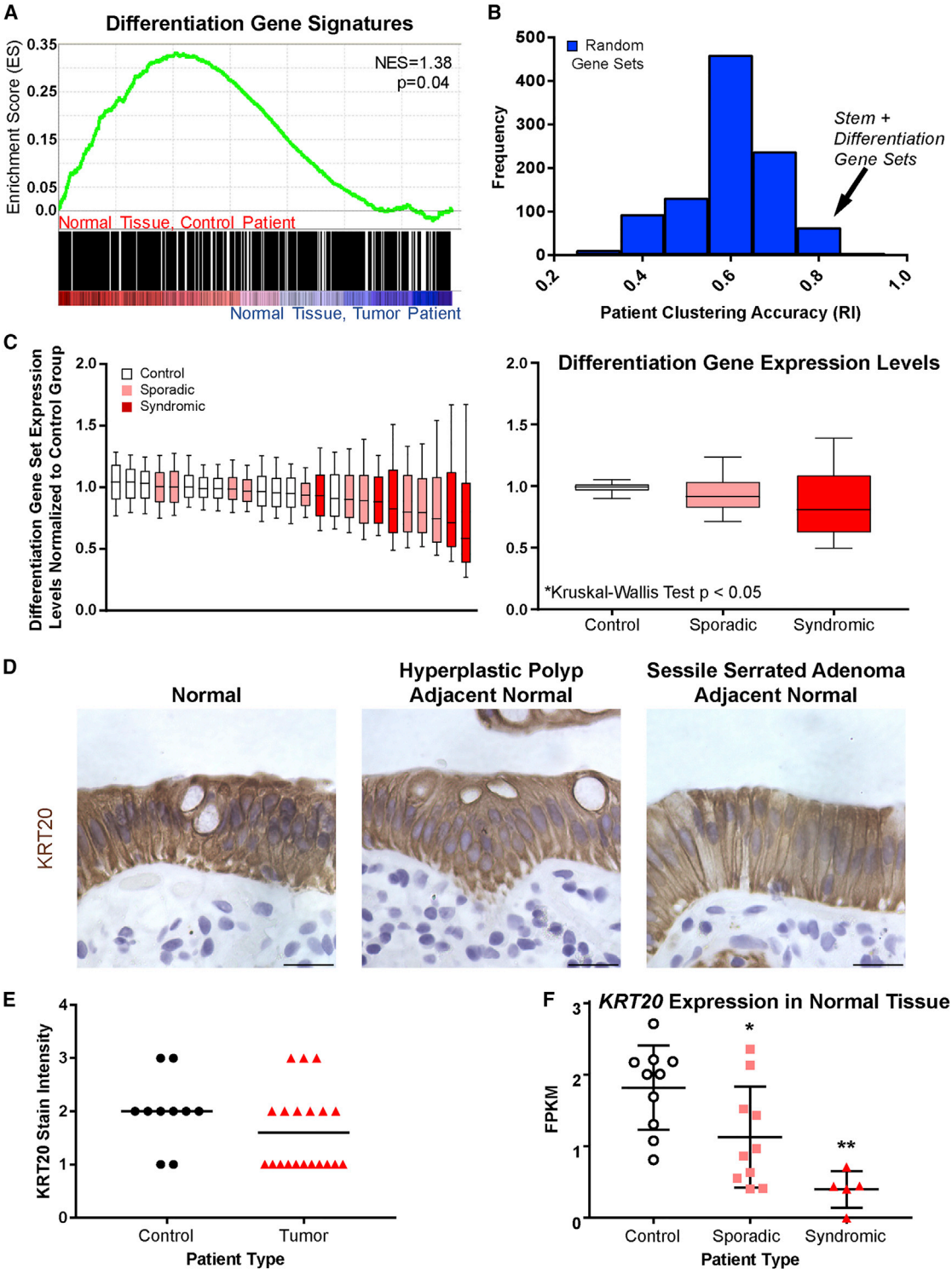

Figure 7. Differentiation Gene Expression Levels in Normal Tissues Corresponds to Serrated Tumor Susceptibility in Humans

(A) Non-tumor, right colon tissue from serrated tumor patients (n = 15) exhibit lower levels of differentiation-gene expression when compared to control patient tissues (n = 10, K-S test).

(B) K-means clustering of patients into tumor and non-tumor classes is improved when combining intestinal stem (Muñoz et al., 2012) and differentiation cell (Chong et al., 2009) gene sets that are differentially regulated in mouse models (performing in the top 2.5% of 1000 random gene lists of equivalent size) or by either gene set individually (Figure S6).

(legend continued on next page)

RI = 0.64) (Rand, 1971). Gene expression levels of stem and differentiation genes were indeed a robust classifier for stratifying patients into tumor and non-tumor groups when compared against the clustering accuracy of random gene panels of equal size (RI = 0.8, scoring in the top 2.5%) (Figure 7B; Table S2). Notably, clustering was more accurate using the combined gene list than either gene set alone (Figure S6). Thus, it appears that the normal epithelium of serrated tumor patients has a shift in the stem-differentiation homeostasis, as was observed in our mouse models. Analysis of individual patient samples revealed that normal patients had relatively higher expression levels of differentiation genes in the right colon tissue when compared with normal tissue from tumor patients (with patients bearing multiple serrated lesions exhibiting the lowest levels of differentiation gene expression)—further suggesting a correlation between tissue differentiation and tumor susceptibility in humans (Figures 7C and 7D, Kruskal-Wallis test, $p < 0.05$). To corroborate these findings, we scored a separate set of patients bearing hyperplastic polyps and sessile serrated adenomas for the protein expression level of KRT20 in adjacent, non-tumor tissue (Figure 7D). Based on blind assessment of KRT20 stain intensity, tumor-bearing patients exhibited a trend toward lower levels of this differentiation marker (Figure 4E, Mann-Whitney U, $p = 0.13362$). Reduced levels of transcripts for *KRT20* were also observed in the normal tissues of patients bearing serrated tumors compared to controls (Figure 7F, ANOVA, $p < 0.05$). Taken together, this study indicates that the human population exhibits a range of differentiation, and an inverse correlation exists between the degree of differentiation and the propensity to develop serrated tumors, echoing the findings in mice described above.

DISCUSSION

Despite the ample genomic characterization of BRAF-driven tumors in human CRCs, few animal studies describe the cellular mechanisms driving serrated tumor initiation. An initial $BRAF^{V600E}$ tumorigenesis model recapitulated some characteristics of human serrated tumors, but mice died prematurely due to several tumors that developed outside the intestine (Carragher et al., 2010). In that study, conditional activation of $BRAF^{V600E}$ in the small intestine resulted in induction of senescence, while tumorigenesis required repression of senescence (Carragher et al., 2010; Kriegl et al., 2011). In contrast, other mouse models of BRAF activation have not found evidence of senescence or apoptosis in the intestine (Rad et al., 2013; Riemer et al., 2015). To better understand the magnitude of MAPK signal influence in CRC initiation, we employed both $BRAF^{V600E}$ heterozygous and homozygous mutants, targeted at the endogenous locus, and initiated in the adult epithelium. Our allelic series revealed that a single allele of mutant BRAF expression is tolerated in the epithelium, but higher levels of MAPK signaling are not tolerated and trigger activation of p21 expression. Together, these results are in agreement with the observed mutual exclusivity of BRAF and KRAS in CRC (Cancer Genome Atlas, 2012; Unni et al., 2015). We propose a model in which only a narrow window of MAPK pathway activity is oncogenic: excessive and early MAPK pathway activation is not tolerated by individual stem cells under normal conditions (such as in $Braf^{V600E}$; $Lgr5\text{-}Cre^{ERT2}$), whereas baseline MAPK levels are not sufficient to promote oncogenesis (such as in control mice). Our work shows that altering the pre-existing differentiation status of a tissue is one factor that modulates tissue tolerance to BRAF activity, essentially expanding the "sweet spot" at which BRAF-driven oncogenesis can occur. Thus, individuals with lower levels of tissue differentiation (whether due to genetic or environmental factors) would have stem cells that are more tolerant to MAPK-activity spikes and are more susceptible to serrated tumorigenesis.

Given that activating mutations of the MAPK pathway drive serrated tumorigenesis in up to 30% of CRC, it is counterintuitive that this pathway would promote differentiation under normal conditions. In our study, stem cells were resistant to retaining oncogenic $BRAF^{V600E}$, unless differentiation-promoting factors were diminished or deleted. These findings suggest the interesting possibility that tissue-resident stem cells evolved a defense mechanism to differentiate in response to oncogenic levels of signaling. This strategy would be particularly appealing in renewing tissues such as the colon, in which all non-stem cell lineages are immediately fated to death as they transit toward the lumen, where they will ultimately be expelled from the epithelium. The mechanism through which $BRAF^{V600E}$ triggers stem cell differentiation is unclear, and whether differentiation is a cause, consequence, or unrelated to p21 activation is also uncertain. Future studies unraveling these mechanisms could provide new opportunities for chemosuppression.

Finally, we show that a normal tissue biopsy can be screened for gene signatures of stem-to-differentiation homeostasis, and this signature can help classify serrated tumor patients versus unaffected individuals. We therefore suggest the possibility that an otherwise healthy mucosa contains a predictive signature for serrated tumor susceptibility. The observation that differentiation status of the human transcriptome is correlated with serrated tumor susceptibility offers exciting opportunities to determine whether gene expression signatures could serve as diagnostics to direct screening practices and whether chemoprevention or dietary strategies could be calibrated to promote a more differentiated epithelium in patients at increased susceptibility to SSA.

EXPERIMENTAL PROCEDURES

Animals and Tissue Processing

Animal experiments were conducted in accordance with Rutgers University IACUC. Mice strains are listed in Table S1. Mice 6 weeks of age were treated

(C) Patients exhibit a range of differentiation gene expression, with serrated cancer patients exhibiting lower levels of intestinal differentiation genes (K-W test, $p < 0.05$). Box and whisker plots of the 5-95th percentile.
(D) Human tissue samples assessed for differentiation marker KRT20 stain intensity.
(E) Adjacent normal tissue of serrated tumor patients exhibits a trend toward reduced stain intensity relative to non-tumor patients (Mann-Whitney, $p = 0.13362$).
(F) *KRT20* transcript levels in normal tissue is lower in serrated tumor patients when compared to non-tumor patient samples (ANOVA, $p < 0.05$). Scale bars, 50 μm.

with intraperitoneal injection of tamoxifen (1 mg/20 g), for 4 consecutive days. Both males and females were used in equal consideration and littermates were used when available for matched experimental sets. Day 1 is considered the onset of treatment, and most animals were investigated at day 5 or at the indicated time point. Mouse intestines were collected and fixed in 4% paraformaldehyde solution overnight at 4°C, and paraffin sections (5 μm) were generated.

For cryo-embedding, the proximal one-third of duodenum was fixed in 4% (v/v) paraformaldehyde overnight at 4°C, washed in cold PBS, and equilibrated in 30% (w/v) sucrose before freezing in OCT compound (catalog no. 4583; Tissue-Tek).

Immunohistochemistry

Slides were treated with 10 mM sodium citrate, and a pressure cooker was used for antigen retrieval. Slides were quenched in 0.5% peroxidase for 20 min, washed, permeabilized in 5% Triton X-100 (in 1× PBS) for 5 min, blocked in 5% FBS for 1 hr, and incubated overnight at 4°C with primary antibodies (Table S3). Slides were developed using 0.05% DAB and 0.015% hydrogen peroxide in 0.1 M Tris, after employing secondary antibody and the ABC Vectastain HRP Kit (Vector Labs), and counterstained with hematoxylin.

Immunofluorescence

10-μm sections of cryo-embedded tissues were examined by direct fluorescence for EGFP expression in Lgr5^{+} stem cells and DAPI for nuclei. Zeiss Axiovert 200M was used for fluorescence microscopy using Retiga-SRV CCD (Q-Imaging). Adjustments to contrast and sharpness, when made, were applied to all images using ImageJ (NIH).

Histochemistry and Scoring

Alkaline phosphatase activity was carried out using the AP Staining Kit II (Stemgent). To detect mucin, rehydrated slides were immersed in 1% Alcian blue solution in 3% aqueous acetic acid (pH 2.5) followed by neutral red counterstain.

Microscopic tumors were quantified based on proliferation markers and morphology, exploring the same tissue space in each mouse, from Swiss roll sections containing the entire gut length. Ki67 staining facilitated identification of these lesions. Dysplasia included regions exhibiting proliferation ¼ of the way above the crypts and higher with major morphological changes including atypical branching or hypervesicular mucinous cells. Carcinomas were classified based on an invasive phenotype with a definite morphologic change in the cells as well as a disturbance of the muscle layer in which proliferation spread past the normal epithelial boundary.

Organoid Forming Assays

Crypt-derived organoids were isolated from duodenum and cultured in Cultrex reduced growth factor matrix R1 (Trevigen) according to established methods (Sato et al., 2009). An average of 100 crypts per biological replicate were seeded in 12.5 μL of matrix with basic crypt media (BCM): advanced DMEM/F12 (GIBCO), 1× penicillin/streptomycin, 2 mM glutamax,10 mM HEPES (Life Technologies) supplemented with 50 ng mL-1EGF (R&D), 100 ng mL-1 Noggin (Peprotech), *N*-acetyl-l-cysteine 1 μM (Sigma-Aldrich), R-Spondin CM 2.5% (v/v), 1× N2, 1× B27 (both from Life Technologies). For rescue experiments of *BRAF*$^{V600E/+}$ organoids, growth media was supplemented with 3 μM CHIR99021 (Stemgent) or Wnt3a-conditioned media (Willert et al., 2003) at 50% (v/v). For WNT inhibition experiments, duodenal crypts were embedded in matrix and passaged after 7 days with 1× TrypLE (GIBCO). Mature organoids were treated with IWP-2, XAV-939 (Tocris), or DMSO vehicle dissolved in complete growth media and changed every 2 days. Organoids were imaged using an AxioVert 200M inverted microscope (Zeiss) with a Retiga-SRV CCD (QImaging).

Cell Culture

Wnt3A-conditioned medium was produced using Wnt3A-expressing L cells (ATCC) cultured in advanced DMEM F/12 supplemented with 10% fetal bovine serum, 2 mM GlutaMAX-I, and 10 mM HEPES (Life Technologies) as previously described (Farin et al., 2016; Willert et al., 2003).

BRAF^{V600E} Recombination Assay

PCR was conducted on isolated intestinal crypt DNA using the primers previously described (Dankort et al., 2007) to resolve wild-type, mutant, and recombined alleles.

Human Colon Tissue KRT20 Analysis

The human study was approved by University Medical Center of Princeton IRB. Immunohistochemical studies on the de-identified normal (n = 10), HPP (n = 10), and SSA (n = 10) used human tissues fixed in 10% neutral formalin and cut to 4 μm at a College of American Pathologists-accredited histology lab. Slides were stained for KRT20 as described above. Non-tumor tissue adjacent to the lesions (HPP or SSA) were imaged and assigned a randomly generated number (1–30). 6 coauthors independently scored KRT20 stain intensity ("light" = 1, "medium" = 2, "dark" = 3) in a blinded fashion. The sum of the 6 scores of each sample was used as the sample's composite score for statistical analyses. Mann-Whitney U (Wilcoxon rank-sum) was used to determine the difference in KRT20 stain intensity.

RNA Sequencing Data Analysis

Mouse intestinal crypts were isolated and processed for RNA using Trizol and sequenced using Illumina's TruSeq RNA Library Prep kit v2 RNA reads were aligned using TopHat2 (v2.1.0). All files were run together using CuffNorm (v2.2.1) using default settings (geometric normalization) (Langmead and Salzberg, 2012; Trapnell et al., 2010). For GSEA analysis, genes were pre-ranked based on signal-to-noise values, as described (Subramanian et al., 2005).

Human data comprising RNA sequencing (RNA-seq) from 25 right colon samples (10 control patients, 10 sporadic SSA tumor patients, and 5 syndromic tumor patients) was derived from non-tumor tissue (Delker et al., 2014; Kanth et al., 2016) (GSE76987). Fragments per kilobase million (FPKM) table was normalized by fold change to the average of the 10 control patient FPKM values for each gene. Specific genes associated with intestinal stem cell and differentiation gene signatures were selected and plotted in R (Chong et al., 2009; Muñoz et al., 2012). Kruskal-Wallis test was performed to determine significant differences between the control, sporadic, and syndromic patients overall.

Differentiation signature genes (Chong et al., 2009) and stem cell signature genes (Muñoz et al., 2012) that were represented on the human RNA-seq FPKM table (GSE76987) (Delker et al., 2014; Kanth et al., 2016) were combined (Table S2), and k-means clustering was performed in R. K-means clustering was performed (clustering of 2) in R, and clustering accuracy was determined using Rand index (RI) (Rand, 1971), RI = (TP + TN)/(TP + TN + FP + FN). Random gene sets, comprised of an equivalent number of unique genes to our defined gene lists, were selected to establish the ability of random classifiers to stratify patients and applied 1,000 times. Distribution frequencies were plotted using 0.1 bin sizes.

Statistical Analyses Performed

Student's t test was used as part of our mouse RNA-seq analyses, Mann-Whitney test was used on blind assessment of human tissue samples, Kruskal Wallis test was used as part of our human RNA-seq data analysis, and Kolmogorov-Smirnov (K-S) test was used on GSEA.

DATA AND SOFTWARE AVAILABILITY

The accession numbers for the RNA-seq files reported in this paper are GEO: GSE106330 and GSE102171. The accession number for the human RNA-seq samples reported in this paper is GEO: GSE76987.

SUPPLEMENTAL INFORMATION

Supplemental Information includes six figures, and three tables and can be found with this article online at https://doi.org/10.1016/j.celrep.2017.11.104.

ACKNOWLEDGMENTS

The authors would like to thank members of the Verzi lab, Dr. David Axelrod, Dr. Ronald Hart, and Dr. Ramesh Shivdasani for their constructive feedback

and discussions. This work was supported by NCI R01CA190558 and a grant from the Human Genetics Institute of New Jersey (to M.P.V.). K.T., O.P.-C., and A.O.P. were supported by New Jersey Commission on Cancer Research (DHFS16PPC036 to K.T., DHSFS17PPC020 to O.P.-C, DFHS13PPC034 to A.O.P.). V.R.S. was supported by the Human Genetics Institute of New Jersey, Summer Undergraduate Research Fellowship. O.A.K. was supported by the Aresty Research Center for Undergraduates. M.P.V. is a member of the Intestinal Stem Cell Consortium, supported by NIDDK and NIAID (U01DK103141), and a member of the Cancer Institute of New Jersey (P30CA072720). The work was supported by an Initiative for Multidisciplinary Research Teams award from Rutgers University, Newark, NJ (to M.P.V. and L.Z.).

AUTHOR CONTRIBUTIONS

Experimental planning and execution were done by M.P.V., O.P.-C., and K.T. Writing was done by M.P.V., O.P.-C., and K.T. All authors contributed to benchwork. Animal husbandry was performed by K.T., O.P.-C., A.O.P., V.R.S., B.N.W., and O.A.K. Computational analysis was performed by M.P.V., O.P.-C., K.T., A.Z., J.X., J.K.T., and R.L.F. Human tissue samples were provided by L.Z. Blind assessment of the KRT20 staining was provided by M.P.V., O.P.-C., K.T., V.R.S., B.N.W., and O.A.K. Human staining data were analyzed by L.Z. and K.T.

DECLARATION OF INTERESTS

The authors declare no competing interests.

Received: August 9, 2017
Revised: November 9, 2017
Accepted: November 29, 2017
Published: December 26, 2017

REFERENCES

Bae, J.M., Lee, T.H., Cho, N.Y., Kim, T.Y., and Kang, G.H. (2015). Loss of CDX2 expression is associated with poor prognosis in colorectal cancer patients. World J. Gastroenterol. *21*, 1457–1467.

Barker, N., van Es, J.H., Kuipers, J., Kujala, P., van den Born, M., Cozijnsen, M., Haegebarth, A., Korving, J., Begthel, H., Peters, P.J., and Clevers, H. (2007). Identification of stem cells in small intestine and colon by marker gene Lgr5. Nature *449*, 1003–1007.

Barker, N., Ridgway, R.A., van Es, J.H., van de Wetering, M., Begthel, H., van den Born, M., Danenberg, E., Clarke, A.R., Sansom, O.J., and Clevers, H. (2009). Crypt stem cells as the cells-of-origin of intestinal cancer. Nature *457*, 608–611.

Cancer Genome Atlas, N.; Cancer Genome Atlas Network (2012). Comprehensive molecular characterization of human colon and rectal cancer. Nature *487*, 330–337.

Carragher, L.A., Snell, K.R., Giblett, S.M., Aldridge, V.S., Patel, B., Cook, S.J., Winton, D.J., Marais, R., and Pritchard, C.A. (2010). V600EBraf induces gastrointestinal crypt senescence and promotes tumour progression through enhanced CpG methylation of p16INK4a. EMBO Mol. Med. *2*, 458–471.

Chong, J.L., Wenzel, P.L., Sáenz-Robles, M.T., Nair, V., Ferrey, A., Hagan, J.P., Gomez, Y.M., Sharma, N., Chen, H.Z., Ouseph, M., et al. (2009). E2f1-3 switch from activators in progenitor cells to repressors in differentiating cells. Nature *462*, 930–934.

Clevers, H. (2013). The intestinal crypt, a prototype stem cell compartment. Cell *154*, 274–284.

Clevers, H., and Nusse, R. (2012). Wnt/β-catenin signaling and disease. Cell *149*, 1192–1205.

Dalerba, P., Sahoo, D., Paik, S., Guo, X., Yothers, G., Song, N., Wilcox-Fogel, N., Forgó, E., Rajendran, P.S., Miranda, S.P., et al. (2016). CDX2 as a prognostic biomarker in stage II and stage III colon cancer. N. Engl. J. Med. *374*, 211–222.

Dankort, D., Filenova, E., Collado, M., Serrano, M., Jones, K., and McMahon, M. (2007). A new mouse model to explore the initiation, progression, and therapy of BRAFV600E-induced lung tumors. Genes Dev. *21*, 379–384.

De Sousa E Melo, F., Wang, X., Jansen, M., Fessler, E., Trinh, A., de Rooij, L.P., de Jong, J.H., de Boer, O.J., van Leersum, R., Bijlsma, M.F., et al. (2013). Poor-prognosis colon cancer is defined by a molecularly distinct subtype and develops from serrated precursor lesions. Nat. Med. *19*, 614–618.

Delker, D.A., McGettigan, B.M., Kanth, P., Pop, S., Neklason, D.W., Bronner, M.P., Burt, R.W., and Hagedorn, C.H. (2014). RNA sequencing of sessile serrated colon polyps identifies differentially expressed genes and immunohistochemical markers. PLoS ONE *9*, e88367.

Dhomen, N., Reis-Filho, J.S., da Rocha Dias, S., Hayward, R., Savage, K., Delmas, V., Larue, L., Pritchard, C., and Marais, R. (2009). Oncogenic Braf induces melanocyte senescence and melanoma in mice. Cancer Cell *15*, 294–303.

Durand, A., Donahue, B., Peignon, G., Letourneur, F., Cagnard, N., Slomianny, C., Perret, C., Shroyer, N.F., and Romagnolo, B. (2012). Functional intestinal stem cells after Paneth cell ablation induced by the loss of transcription factor Math1 (Atoh1). Proc. Natl. Acad. Sci. USA *109*, 8965–8970.

el Marjou, F., Janssen, K.P., Chang, B.H., Li, M., Hindie, V., Chan, L., Louvard, D., Chambon, P., Metzger, D., and Robine, S. (2004). Tissue-specific and inducible Cre-mediated recombination in the gut epithelium. Genesis *39*, 186–193.

Farin, H.F., Jordens, I., Mosa, M.H., Basak, O., Korving, J., Tauriello, D.V., de Punder, K., Angers, S., Peters, P.J., Maurice, M.M., and Clevers, H. (2016). Visualization of a short-range Wnt gradient in the intestinal stem-cell niche. Nature *530*, 340–343.

Fearon, E.R. (2011). Molecular genetics of colorectal cancer. Annu. Rev. Pathol. *6*, 479–507.

Fearon, E.R., and Vogelstein, B. (1990). A genetic model for colorectal tumorigenesis. Cell *61*, 759–767.

Guo, R.J., Funakoshi, S., Lee, H.H., Kong, J., and Lynch, J.P. (2010). The intestine-specific transcription factor Cdx2 inhibits beta-catenin/TCF transcriptional activity by disrupting the beta-catenin-TCF protein complex. Carcinogenesis *31*, 159–166.

Harada, N., Tamai, Y., Ishikawa, T., Sauer, B., Takaku, K., Oshima, M., and Taketo, M.M. (1999). Intestinal polyposis in mice with a dominant stable mutation of the beta-catenin gene. EMBO J. *18*, 5931–5942.

Hazewinkel, Y., López-Cerón, M., East, J.E., Rastogi, A., Pellisé, M., Nakajima, T., van Eeden, S., Tytgat, K.M., Fockens, P., and Dekker, E. (2013). Endoscopic features of sessile serrated adenomas: validation by international experts using high-resolution white-light endoscopy and narrow-band imaging. Gastrointest. Endosc. *77*, 916–924.

Kabiri, Z., Greicius, G., Madan, B., Biechele, S., Zhong, Z., Zaribafzadeh, H., Edison, Aliyev, J., Wu, Y., Bunte, R., et al. (2014). Stroma provides an intestinal stem cell niche in the absence of epithelial Wnts. Development *141*, 2206–2215.

Kanth, P., Bronner, M.P., Boucher, K.M., Burt, R.W., Neklason, D.W., Hagedorn, C.H., and Delker, D.A. (2016). Gene signature in sessile serrated polyps identifies colon cancer subtype. Cancer Prev. Res. (Phila.) *9*, 456–465.

Kim, T.H., Escudero, S., and Shivdasani, R.A. (2012). Intact function of Lgr5 receptor-expressing intestinal stem cells in the absence of Paneth cells. Proc. Natl. Acad. Sci. USA *109*, 3932–3937.

Kriegl, L., Neumann, J., Vieth, M., Greten, F.R., Reu, S., Jung, A., and Kirchner, T. (2011). Up and downregulation of p16(Ink4a) expression in BRAF-mutated polyps/adenomas indicates a senescence barrier in the serrated route to colon cancer. Mod. Pathol *24*, 1015–1022.

Landau, M.S., Kuan, S.F., Chiosea, S., and Pai, R.K. (2014). BRAF-mutated microsatellite stable colorectal carcinoma: an aggressive adenocarcinoma with reduced CDX2 and increased cytokeratin 7 immunohistochemical expression. Hum. Pathol. *45*, 1704–1712.

Langmead, B., and Salzberg, S.L. (2012). Fast gapped-read alignment with Bowtie 2. Nat. Methods *9*, 357–359.

Leggett, B., and Whitehall, V. (2010). Role of the serrated pathway in colorectal cancer pathogenesis. Gastroenterology *138*, 2088–2100.

Liu, X., Zhang, X., Zhan, Q., Brock, M.V., Herman, J.G., and Guo, M. (2012). CDX2 serves as a Wnt signaling inhibitor and is frequently methylated in lung cancer. Cancer Biol. Ther. *13*, 1152–1157.

Muñoz, J., Stange, D.E., Schepers, A.G., van de Wetering, M., Koo, B.K., Itzkovitz, S., Volckmann, R., Kung, K.S., Koster, J., Radulescu, S., et al. (2012). The Lgr5 intestinal stem cell signature: robust expression of proposed quiescent '+4′ cell markers. EMBO J. *31*, 3079–3091.

Mutoh, H., Hakamata, Y., Sato, K., Eda, A., Yanaka, I., Honda, S., Osawa, H., Kaneko, Y., and Sugano, K. (2002). Conversion of gastric mucosa to intestinal metaplasia in Cdx2-expressing transgenic mice. Biochem. Biophys. Res. Commun. *294*, 470–479.

Powell, S.M., Zilz, N., Beazer-Barclay, Y., Bryan, T.M., Hamilton, S.R., Thibodeau, S.N., Vogelstein, B., and Kinzler, K.W. (1992). APC mutations occur early during colorectal tumorigenesis. Nature *359*, 235–237.

Rad, R., Cadiñanos, J., Rad, L., Varela, I., Strong, A., Kriegl, L., Constantino-Casas, F., Eser, S., Hieber, M., Seidler, B., et al. (2013). A genetic progression model of Braf(V600E)-induced intestinal tumorigenesis reveals targets for therapeutic intervention. Cancer Cell *24*, 15–29.

Rand, W.M. (1971). Objective criteria for the evaluation of clustering methods. J. Am. Stat. Assoc. *66*, 846–850.

Rex, D.K., Ahnen, D.J., Baron, J.A., Batts, K.P., Burke, C.A., Burt, R.W., Goldblum, J.R., Guillem, J.G., Kahi, C.J., Kalady, M.F., et al. (2012). Serrated lesions of the colorectum: review and recommendations from an expert panel. Am. J. Gastroenterol. *107*, 1315–1329.

Riemer, P., Sreekumar, A., Reinke, S., Rad, R., Schäfer, R., Sers, C., Bläker, H., Herrmann, B.G., and Morkel, M. (2015). Transgenic expression of oncogenic BRAF induces loss of stem cells in the mouse intestine, which is antagonized by β-catenin activity. Oncogene *34*, 3164–3175.

Sakamoto, N., Feng, Y., Stolfi, C., Kurosu, Y., Green, M., Lin, J., Green, M.E., Sentani, K., Yasui, W., McMahon, M., et al. (2017). BRAFV600E cooperates with CDX2 inactivation to promote serrated colorectal tumorigenesis. eLife *6*, e20331.

Sato, T., Vries, R.G., Snippert, H.J., van de Wetering, M., Barker, N., Stange, D.E., van Es, J.H., Abo, A., Kujala, P., Peters, P.J., and Clevers, H. (2009). Single Lgr5 stem cells build crypt-villus structures in vitro without a mesenchymal niche. Nature *459*, 262–265.

Sekine, S., Yamashita, S., Tanabe, T., Hashimoto, T., Yoshida, H., Taniguchi, H., Kojima, M., Shinmura, K., Saito, Y., Hiraoka, N., et al. (2016). Frequent PTPRK-RSPO3 fusions and RNF43 mutations in colorectal traditional serrated adenoma. J. Pathol. *239*, 133–138.

Silberg, D.G., Sullivan, J., Kang, E., Swain, G.P., Moffett, J., Sund, N.J., Sackett, S.D., and Kaestner, K.H. (2002). Cdx2 ectopic expression induces gastric intestinal metaplasia in transgenic mice. Gastroenterology *122*, 689–696.

Stringer, E.J., Duluc, I., Saandi, T., Davidson, I., Bialecka, M., Sato, T., Barker, N., Clevers, H., Pritchard, C.A., Winton, D.J., et al. (2012). Cdx2 determines the fate of postnatal intestinal endoderm. Development *139*, 465–474.

Subramanian, A., Tamayo, P., Mootha, V.K., Mukherjee, S., Ebert, B.L., Gillette, M.A., Paulovich, A., Pomeroy, S.L., Golub, T.R., Lander, E.S., and Mesirov, J.P. (2005). Gene set enrichment analysis: a knowledge-based approach for interpreting genome-wide expression profiles. Proc. Natl. Acad. Sci. USA *102*, 15545–15550.

Suh, E., and Traber, P.G. (1996). An intestine-specific homeobox gene regulates proliferation and differentiation. Mol. Cell. Biol. *16*, 619–625.

Tian, X., Du, H., Fu, X., Li, K., Li, A., and Zhang, Y. (2009). Smad4 restoration leads to a suppression of Wnt/beta-catenin signaling activity and migration capacity in human colon carcinoma cells. Biochem. Biophys. Res. Commun. *380*, 478–483.

Trapnell, C., Williams, B.A., Pertea, G., Mortazavi, A., Kwan, G., van Baren, M.J., Salzberg, S.L., Wold, B.J., and Pachter, L. (2010). Transcript assembly and quantification by RNA-Seq reveals unannotated transcripts and isoform switching during cell differentiation. Nat. Biotechnol. *28*, 511–515.

Unni, A.M., Lockwood, W.W., Zejnullahu, K., Lee-Lin, S.Q., and Varmus, H. (2015). Evidence that synthetic lethality underlies the mutual exclusivity of oncogenic KRAS and EGFR mutations in lung adenocarcinoma. eLife *4*, e06907.

Van der Flier, L.G., Sabates-Bellver, J., Oving, I., Haegebarth, A., De Palo, M., Anti, M., Van Gijn, M.E., Suijkerbuijk, S., Van de Wetering, M., Marra, G., and Clevers, H. (2007). The intestinal Wnt/TCF signature. Gastroenterology *132*, 628–632.

Verzi, M.P., Shin, H., He, H.H., Sulahian, R., Meyer, C.A., Montgomery, R.K., Fleet, J.C., Brown, M., Liu, X.S., and Shivdasani, R.A. (2010). Differentiation-specific histone modifications reveal dynamic chromatin interactions and partners for the intestinal transcription factor CDX2. Dev. Cell *19*, 713–726.

Visvader, J.E. (2011). Cells of origin in cancer. Nature *469*, 314–322.

Willert, K., Brown, J.D., Danenberg, E., Duncan, A.W., Weissman, I.L., Reya, T., Yates, J.R., 3rd, and Nusse, R. (2003). Wnt proteins are lipid-modified and can act as stem cell growth factors. Nature *423*, 448–452.

Yang, X., Li, C., Herrera, P.L., and Deng, C.X. (2002). Generation of Smad4/Dpc4 conditional knockout mice. Genesis *32*, 80–81.

Cell Reports, Volume *21*

Supplemental Information

Degree of Tissue Differentiation Dictates Susceptibility to BRAF-Driven Colorectal Cancer

Kevin Tong, Oscar Pellón-Cárdenas, Veerin R. Sirihorachai, Bailey N. Warder, Om A. Kothari, Ansu O. Perekatt, Emily E. Fokas, Robert L. Fullem, Anbo Zhou, Joshua K. Thackray, Hiep Tran, Lanjing Zhang, Jinchuan Xing, and Michael P. Verzi

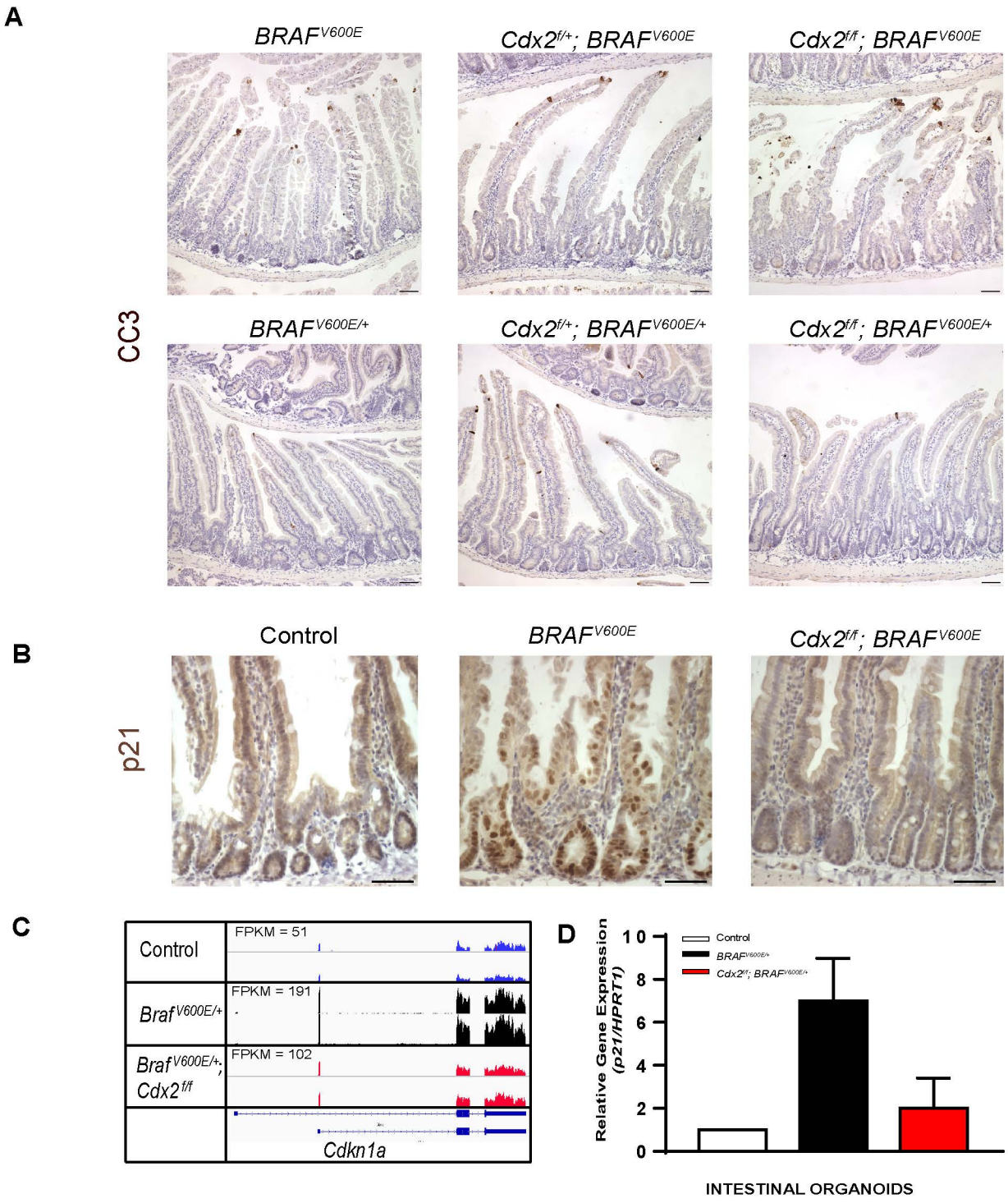

Figure S1. BRAF^{V600E} activation promotes p21 induction in intestinal crypts, Related to Figure 1.

A) BRAF^{V600E} activation does not promote apoptosis in intestinal stem cells. There are no major differences in the localization or frequency of cleaved caspase-3 staining between control mice and mutant mice. Scale bars = 50 μm. B) BRAF^{V600E} activation in a homozygous manner induces accumulation of p21 dependent on CDX2. The induction of p21 was mainly localized to crypt cells and completely absent in the intestine of control and *CDX2$^{f/f}$;BRAF^{V600E}* mice. Scale bars = 50 μm. C) Normalized RNA-seq reads indicate a higher expression of *Cdkn1a* (*p21*) in *Braf$^{V600E/+}$* mice. Upregulation of the *Cdkn1a* predominantly occurs in a CDX2-dependent manner. D) qRT-PCR of *Cdkn1a* (*p21*) in small intestine organoids shows that *Cdx2$^{f/f}$;BRAF$^{V600E/+}$* organoids had reduced levels of p21 expression compared to *BRAF$^{V600E/+}$* organoids after 4 days in culture. Bars represent mean ± SD from two independent experiments.

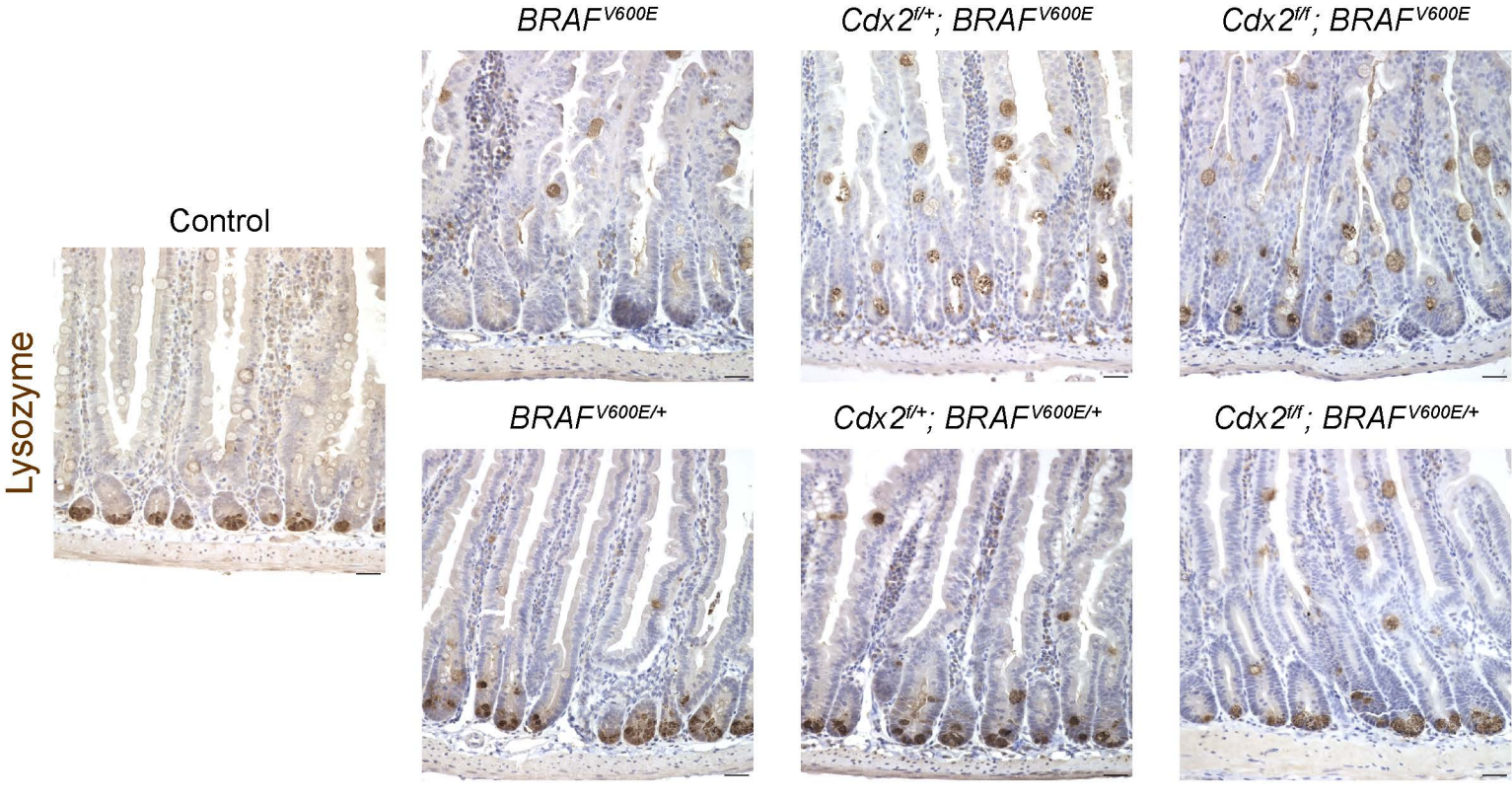

Figure S2. Braf^{V600E} activation triggers Paneth Cell loss, Related to Figure 2.
Paneth cells, as marked by Lysozyme immunostaining, are lost in the Braf^{V600E} crypts, and do not appreciably return upon reduced levels of CDX2. Lysozyme positive cells are found in the villi of both the Braf^{V600E} and Cdx2$^{f/f}$; Braf^{V600E} mutants. These findings are consistent with previous reports indicating that MAPK activation promotes Goblet cell differentiation at the expense of Paneth cells (Heuberger et al., 2014). Scale bars = 50 μm.

FIGURE S3

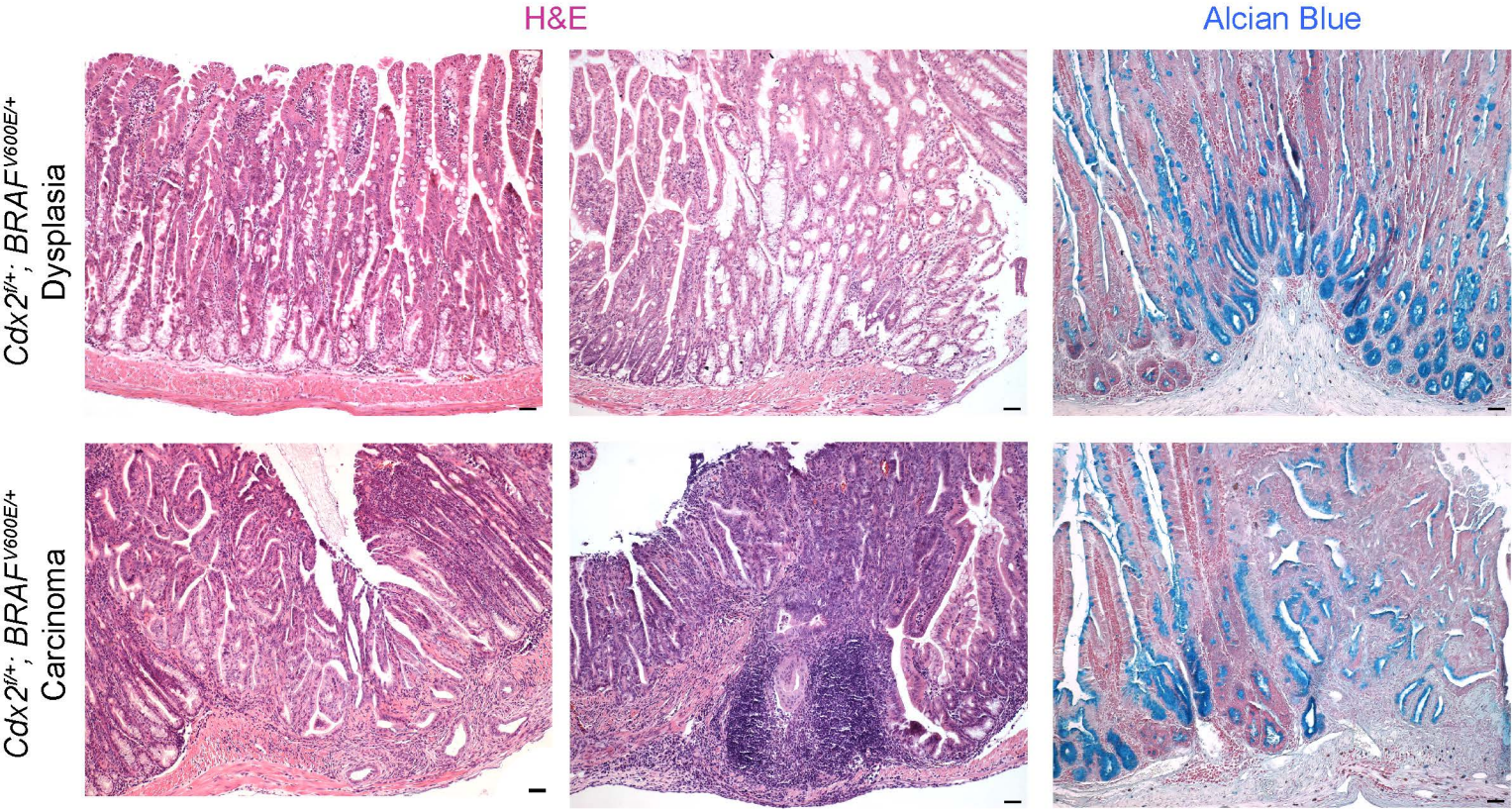

Figure S3. *Cdx2*$^{f/+}$;*BRAF*$^{V600E/+}$ Mice develop serrated tumors, Related to Figure 3.
Cdx2$^{f/+}$; *BRAF*$^{V600E/+}$ compound mutant mice reveal lesions with serrated morphology (H&E) and mature mucinous cells (Alcian Blue) - resembling human hyperplastic polyps and sessile serrated adenomas that predominantly harbor BRAF mutations. This is an expanded set of images to complement those featured in Figure 3. Scale bars = 50 μm.

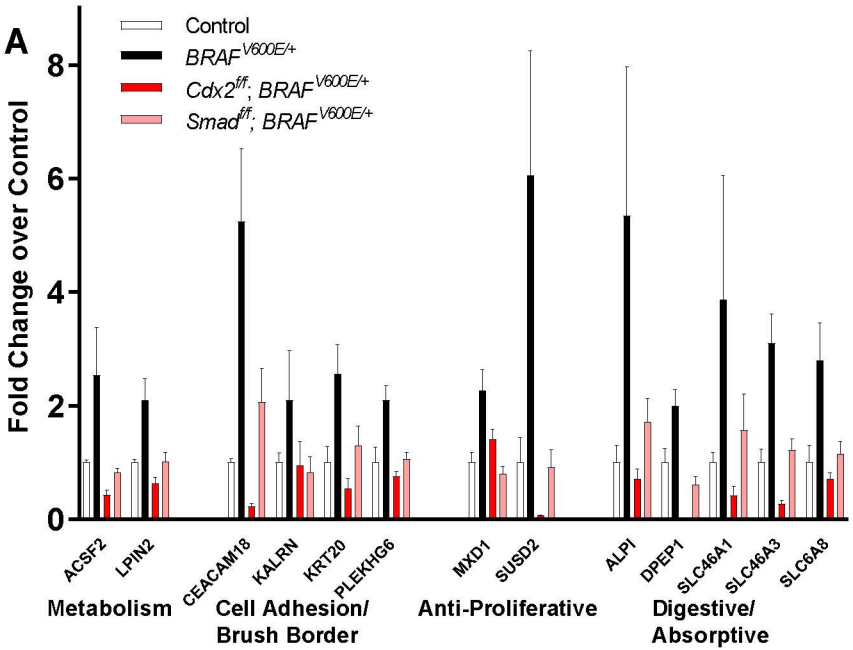

Figure S4. *Smad4* Loss Suppresses Differentiation Genes, Related to Figure 4.
Examples of the types of differentiation-associated genes that are elevated upon BRAF activation, and suppressed upon *Smad4* loss. Control, $BRAF^{V600E/+}$, and $Cdx2^{f/f}$; $BRAF^{V600E/+}$ replicates are the same as previously shown (Figure 2). Bars represent mean ± SD from three independent experiments.

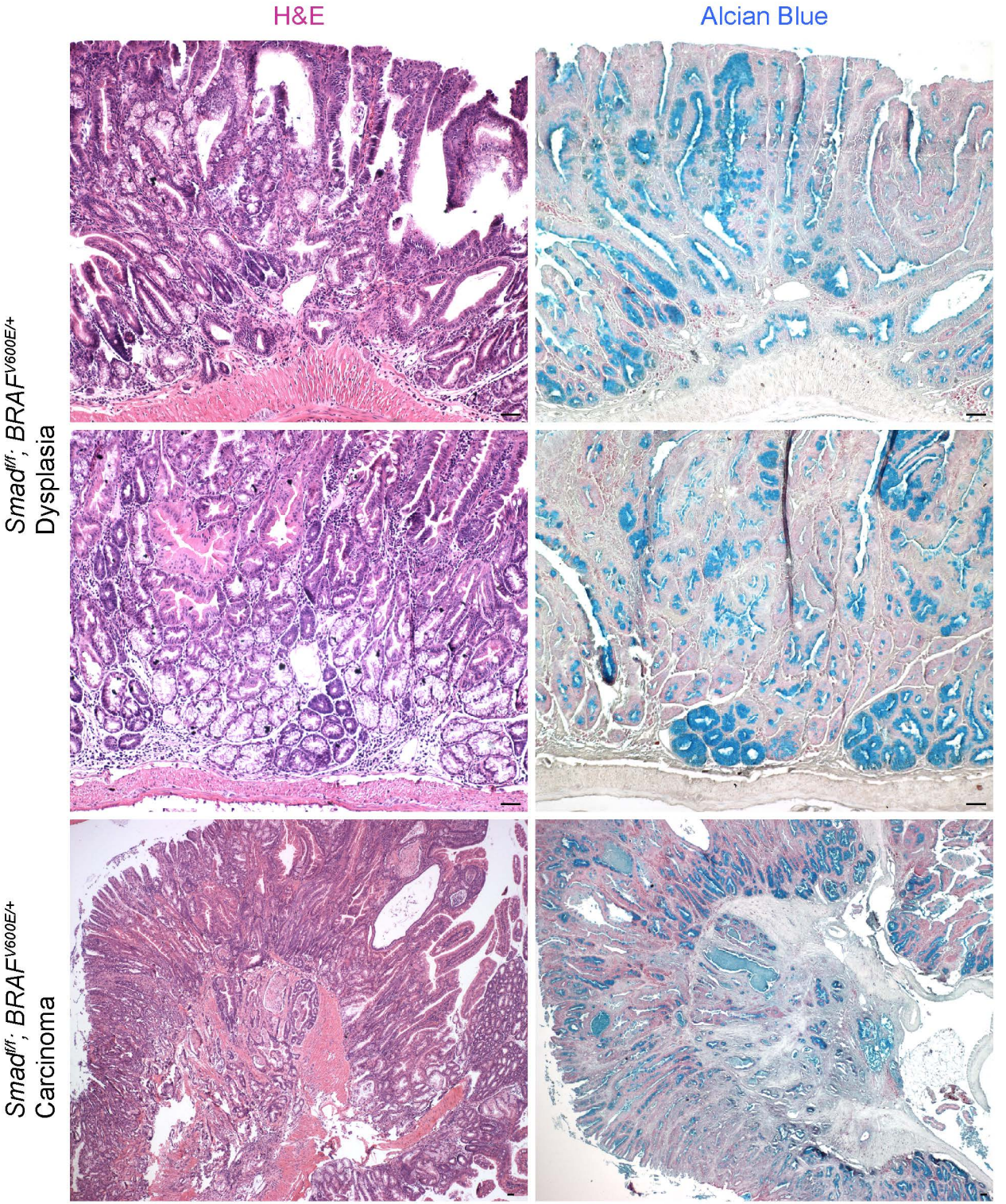

Figure S5. *Smad4*$^{f/f}$*; BRAF*$^{V600E/+}$ mice develop serrated tumors, Related to Figure 5.
Smad4$^{f/f}$*; BRAF*$^{V600E/+}$ mice reveal large, serrated, mucinous dysplasias and carcinomas mirroring the serrated morphology described in *Cdx2*$^{f/+}$*; BRAF*$^{V600E/+}$ mice. Scale bars = 50 μm.

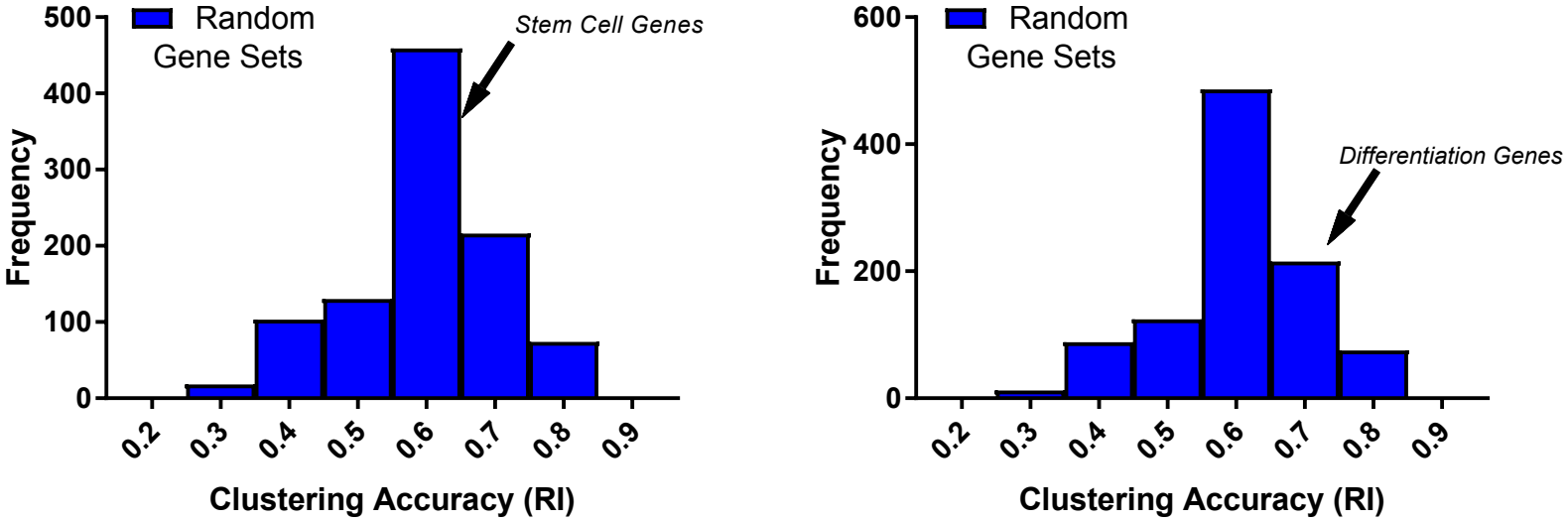

Figure S6. K-means clustering of human patient transcriptomes, based upon Intestinal Stem Cell and Differentiation Gene sets, Related to Figure 7.

K-means clustering of non-tumor, ascending colon tissue from serrated tumor patients (n=15) and control patient tissue (n=10) using intestinal stem (Munoz et al., 2012) and differentiated cell (Chong et al., 2009) gene sets that are also differentially regulated in mouse models (See Figures 1-2), relative to 1000 random gene sets of equivalent size (see Table S2, Figure 7). Neither the stem cell gene set (RI = 0.60), nor the differentiated cell gene set (RI = 0.76) performed as well as the combined gene set in clustering accuracy (Figure 7).

Table S1. Table of transgenic alleles used in this study, Related to Figures 1-6 and Methods.

Allele	Reference
Mouse: *BRAF^{V600E}*	Dankfort et al., 2007
Mouse: *Cdx2^{f}*	Verzi et al., 2012
Mouse: *Lgr5-EGFP-IRES-Cre^{ERT2}*	Barker et al., 2007
Mouse: *Smad4^{f}*	Yang et al., 2002
Mouse: *Villin-Cre^{ERT2}*	el Marjou et al., 2004
Mouse: β-catenin$^{Exon3f/+}$	Harada et al., 1999

Table S3. Antibodies Used in This Study, Related to Figures 1, 2, 4, 6, 7 and Methods.

Antigen	Species	Dilution	Vendor	Catalog Number
Ki67	Rabbit	1:300	Abcam	ab16667, lot: GR52456-1
OLFM4	Rabbit	1:5000	Cell Signaling	39141S, lot: 1
SOX9	Rabbit	1:300	Millipore	AB5535, lot: 2593867
CD44	Rat	1:300	BD	558739, lot: 5212970
CDX2	Rabbit	1:300	Cell Signaling	12306S, lot: 1
CC3	Rabbit	1:200	Cell Signaling	9661S
Lysozyme	Rabbit	1:2000	Dako	A00999
KRT20	Rabbit	1:2700	Cell Signaling	13063, lot:1